

Structure of quasiparticles in a local Fermi liquid

Izak Snyman *Mandelstam Institute for Theoretical Physics, School of Physics, University of the Witwatersrand, Johannesburg, South Africa*

(Received 1 September 2023; revised 24 October 2023; accepted 25 October 2023; published 13 November 2023)

Conduction electrons interacting with a dynamic impurity can give rise to a local Fermi liquid. The latter has the same low-energy spectrum as an ideal Fermi gas containing a static impurity. The Fermi liquids's elementary excitations are, however, not bare electrons. In the vicinity of the impurity, they are dressed by virtual particle-hole pairs. Here we study this dressing. Among other things, we construct a mode-resolved measure of dressing. To evaluate it in position representation, we have to circumvent the limitations of the numerical renormalization group, which discretizes the conduction band logarithmically. We therefore extend natural orbital methods that successfully characterize the ground state, to describe excitations. We demonstrate that the dressing profile shows nontrivial power-law decay at large distances. Our natural orbital methodology could lay the foundation for calculating the properties of local Fermi-liquid quasiparticles in nontrivial geometries such as disordered hosts or mesoscopic devices.

DOI: [10.1103/PhysRevB.108.205120](https://doi.org/10.1103/PhysRevB.108.205120)

I. INTRODUCTION

Fermi liquids emerge near infrared fixed points in the renormalization group flow of some interacting many-fermion systems [1]. There is something alchemical about them. Renormalization plays the role of the philosopher's stone, so that it often remains a mystery how the independent quasiparticles (the proverbial gold) are constituted out of the raw ingredients—bare electrons. Physicists characterize the low-energy behavior of Fermi liquids in terms of a handful of parameters that are determined from experiment. A more daunting task is to determine how the Fermi-liquid parameters depend on the microscopic parameters of a given physical realization.

Local Fermi liquids are a class of systems in which this challenging problem has met with success [2]. They occur in dynamic quantum impurity models, where a small interacting quantum system is coupled to a bulk system of noninteracting fermions. They are interesting many-body systems in their own right [3], and also appear as a key ingredient in dynamical mean field theory [4], an important method in the study of bulk-interacting systems. For these reasons, their dynamics is an active field of study [5–9]. Often, the quantity of interest is the impurity Green's function, and nontrivial methods have been developed, that are geared to calculating it. This exploits the fact that a very precise description of the impurity can be achieved, employing a less precise description of the bulk. The lack of precision where the bulk is concerned, can lead to difficulty, when attempting to study the structure of correlations that live in the bulk [10–15].

The fact that a Fermi-liquid description applies in certain quantum impurity models, was established half a century ago, using the numerical renormalization group (NRG) [16]. This method was able to compute the low-energy many-body spectrum, whose structure was found to be nearly identical to that of a noninteracting fermion system [17–19]. The

spectrum obtained for a given set of microscopic parameters was fitted to a noninteracting fixed point Hamiltonian plus leading irrelevant perturbations. In this way, the microscopic parameters could be mapped to the Fermi-liquid parameters they give rise to [20–23]. This raises a prospect, which seems unfeasible for other Fermi liquids. Can one explicitly calculate how the quasiparticle excitations of a local Fermi liquid are constituted out of bare electronic degrees of freedom? This question is particularly challenging to answer when a dynamic quantum impurity is imbedded in a host in which electrons experience a nontrivial potential landscape, such as disorder, or electrostatic gates [24–32]. Using scanning gate microscopy, experimentalists have succeeded in obtaining a real space picture of quasiparticle excitations in such systems [33–35]. The microscopic modeling of these experiments may benefit from the development of new methods. One reason why NRG is inadequate, is that it discretizes the bulk on what is called a logarithmic energy grid. This throws away short-wavelength information required to achieve good spatial resolution of many-body correlations in the vicinity of the impurity [11,12,36]. A second reason is that NRG discards all but the very lowest single-quasiparticle excitations before their long-wavelength structure is fully resolved [37,38].

Another single-particle-like picture that is distinct from Fermi-liquid theory is important for understanding many-body correlations in the ground states of quantum impurity problems [39,40]. Associated with this picture are a set of bare single-particle orbitals called natural orbitals [41,42]. They form the single-particle basis in which a correlated ground state is expressed as a linear combination of the fewest number of Slater determinants. Natural orbital methods have an established role in quantum chemistry, where they successfully account for chemical properties of strongly correlated few-electron systems [43,44]. There has recently been increased interest in the applications of natural orbital methods in

condensed matter [45,46], including quantum impurity problems [47,48], where high accuracy in very large systems have been achieved at modest computational cost [15]. The present study was inspired by the question as to whether natural orbitals can shed light on the structure of quasiparticle excitations in a local Fermi liquid.

Our main results are as follows. We have developed methods for analyzing single-quasiparticle excitations in a large finite system consisting of a quantum impurity hybridized with a noninteracting host. It clarifies the relationship between the single-particle eigenstates of the noninteracting effective quasiparticle Hamiltonian, and the associated many-body eigenstates of the original interacting Hamiltonian. This connection allows one to split the many-body eigenstate into two parts, corresponding respectively to a bare electron on top of the ground state and to the dressing of the bare electron by particle-hole pairs. We developed an accurate ansatz for single-quasiparticle excitations on top of the ground state in terms of natural orbitals. This allowed us to investigate quasiparticle excitations that are discarded in NRG, and to investigate the structure of the dressing of bare electrons in real space. We could study a bulk consisting of thousands of sites and resolve the wave function with single site precision. We thus obtained results on the nontrivial power-law decay of dressing with distance, that NRG is unable to resolve. Our results could lead to advances in the study of spatial features of low-energy excitations in local Fermi liquids, including the modeling of realistic environments, such as atomic lattices, static disorder, and mesoscopic electronic devices. It could also lead to the further refinement of natural orbital methods to study the dynamics of quantum impurities.

The rest of the article is structured as follows. In Sec. II we introduce the single impurity Anderson model [49], that we will focus on. We review elementary aspects of the local Fermi-liquid theory that applies to it at low energies, and formulate the questions regarding its quasiparticle excitations that guided the present study. We explain the limitations of NRG, and review the natural orbital methods that apply to the study of the model's ground state. In Sec. III we present the theoretical developments that our study contribute to local Fermi-liquid theory. In Sec. IV we employ the theory that we developed in Sec. III to numerically study the structure of single-quasiparticle excitations. Section V contains a summary of our main results, and concluding remarks. As evidence that our natural orbital methods are sufficiently accurate for our purposes, in an appendix we compare to results obtained by other means.

II. BACKGROUND AND AIMS OF THE STUDY

A. Local Fermi-liquid theory and the single impurity Anderson model

In this article, our primary focus will be on the single impurity Anderson model (SIAM) [2,49]. It describes \hat{d}_σ^\dagger electrons in a localized orbital interacting via Coulomb repulsion U and hybridizing with the noninteracting $\hat{c}_{k\sigma}^\dagger$ electrons in a Fermi sea. Here k is an orbital index that may refer to (Bloch) momentum in a uniform system, and $\sigma \in \{\uparrow, \downarrow\}$ denotes spin.

The Hamiltonian reads

$$\hat{H} = U \hat{n}_{d\uparrow} \hat{n}_{d\downarrow} + \varepsilon_d (\hat{n}_{d\uparrow} + \hat{n}_{d\downarrow}) + V \sum_{\sigma} (\hat{d}_{\sigma}^{\dagger} \hat{\psi}_{0\sigma} + \hat{\psi}_{0\sigma}^{\dagger} \hat{d}_{\sigma}) + \sum_{k=1}^L \sum_{\sigma} \varepsilon_k \hat{c}_{k\sigma}^{\dagger} \hat{c}_{k\sigma}, \quad (1)$$

where $\hat{n}_{d\sigma} = \hat{d}_{\sigma}^{\dagger} \hat{d}_{\sigma}$, and $\hat{\psi}_{0\sigma}^{\dagger} = \frac{1}{\sqrt{L}} \sum_{k=1}^L \hat{c}_{k\sigma}^{\dagger}$ creates an electron on the lattice site closest to the impurity. To quantify the hybridization, it is conventional to cite the spectral density

$$\Delta = \pi \nu V^2 \quad (2)$$

at the Fermi level, of the operator $V \hat{\psi}_0$ in the infinite system uncoupled from the impurity, rather than V . In the above expression, ν is the bulk density of states per unit volume at the Fermi level. We measure single-particle energies such that the Fermi energy lies at zero. If $-\varepsilon_d > \Delta$ and $\varepsilon_d + U > \Delta$, the ground-state occupation probability of the d orbital is approximately one, meaning it possesses a spin-1/2 magnetic moment. We will focus on the particle-hole symmetric case, where the energy of the d orbital is tuned such that $\varepsilon_d = -U/2$, and the condition for single occupation of the d orbital becomes $U/2 > \Delta$. Virtual processes in which the singly-occupied impurity is emptied and then reoccupied, or doubly occupied and then returned to single occupancy, lead to an effective antiferromagnetic spin-exchange interaction between the impurity and the band. Kondo physics results, associated with an emergent Kondo scale T_K , given by the inverse of the d orbital's susceptibility to being spin polarized by a local magnetic field

$$T_K = \frac{1}{4\chi}, \quad \chi = \lim_{B \rightarrow 0} \langle (\hat{n}_{d\uparrow} - \hat{n}_{d\downarrow}) \rangle_B / B. \quad (3)$$

Here $\langle \cdots \rangle_B$ denotes the ground-state expectation value when the Hamiltonian is perturbed by the local field

$$\hat{H}_B = \hat{H} - \frac{B}{2} (\hat{n}_{d\uparrow} - \hat{n}_{d\downarrow}). \quad (4)$$

Krishna-Murthy, Wilkins, and Wilson (KWW) [19] showed by means of NRG that the SIAM flows to strong coupling, and reaches a stable infrared fixed point below T_K . At energies sufficiently lower than the Kondo scale, the many-body energy spectrum of the model resembles that of a noninteracting Fermi gas, i.e., it is given by

$$E(\{v_{\alpha\sigma}\}) = \text{const.} + \sum_{\alpha} E_{\alpha} n_{\alpha\sigma}, \quad (5)$$

where the quantum numbers $n_{\alpha\sigma} \in \{0, 1\}$ can be interpreted as the occupation numbers of quasiparticle orbitals. While no explicit mapping relating the low-energy quasiparticles to the bare fermions appearing in Eq. (1) have ever been derived, *a priori* one expects the quasiparticle creation and annihilation operators to be nonlinear functions of the bare fermion operators $\hat{c}_{k\sigma}$, $\hat{c}_{k\sigma}^{\dagger}$, \hat{d}_{σ} , and $\hat{d}_{\sigma}^{\dagger}$. In other words, we expect the quasiparticles to be fermions dressed with particle-hole pairs.

Hewson [20], building on ideas of Nozières [18], also introduced a quasiparticle Hamiltonian for the SIAM, as a starting point for a “renormalized” perturbation theory. Hewson relied on the generic behavior of the (zero-temperature) retarded

self-energy of a class of fermionic models that includes the SIAM, namely that the self-energy can be expanded in frequency around $\omega = 0$,

$$\Sigma(\omega) = \Sigma(0) + \Sigma'(0)\omega + \Sigma^{\text{rem}}(\omega), \quad (6)$$

and that $\Sigma(0)$ and $\Sigma'(0)$ are both real. The interacting retarded Green's function for the d orbital reads $G_{\sigma\sigma'}(\omega) = \delta_{\sigma\sigma'}/(\omega - \varepsilon_d + i\Delta - \Sigma(\omega))$. Hewson rewrote $G_{\sigma\sigma'}(\omega)$ as

$$G_{\sigma\sigma'}(\omega) = \frac{z\delta_{\sigma\sigma'}}{\omega - \tilde{\varepsilon}_d + i\tilde{\Delta} - \tilde{\Sigma}(\omega)}, \quad (7)$$

where $z = 1/[1 - \Sigma'(0)]$, $\tilde{\varepsilon}_d = z[\varepsilon_d + \Sigma(0)]$ and $\tilde{\Sigma}(\omega) = z\Sigma^{\text{rem}}(\omega) \propto \omega^2$. (In the particle-hole symmetric case, $\tilde{\varepsilon}_d = 0$.) At sufficiently low frequencies/energies, $\tilde{\Sigma}(\omega)$ makes a very small contribution to the denominator, and can be neglected. Hewson therefore defined a quasiparticle Hamiltonian \hat{H}_{qp} that has the same form as the noninteracting version of Eq. (1), with $U = 0$. Furthermore, he made the replacements $V \rightarrow \tilde{V} = \sqrt{z}V$ and $\varepsilon_d \rightarrow \tilde{\varepsilon}_d$. If we denote the retarded d orbital Green's function of Hewson's quasiparticle Hamiltonian by $\tilde{G}_{\sigma,\sigma'}(\omega)$, and drop $\tilde{\Sigma}(\omega)$ in the expression (7) for $G_{\sigma\sigma'}(\omega)$, then $G_{\sigma\sigma'}(\omega) = z\tilde{G}_{\sigma\sigma'}(\omega)$. The elastic scattering amplitudes for a bare electrons incident on the impurity are determined by the transfer matrix

$$\begin{aligned} T_{kk'}(\omega) &= \frac{1}{L} \frac{V}{\omega - \varepsilon_k} G_{\sigma\sigma}(\omega) \frac{V}{\omega - \varepsilon_{k'}} \\ &\simeq \frac{1}{L} \frac{\tilde{V}}{\omega - \varepsilon_k} \tilde{G}_{\sigma\sigma}(\omega) \frac{\tilde{V}}{\omega - \varepsilon_{k'}}. \end{aligned} \quad (8)$$

The second line of the above equation implies that at low energies, *bare* electrons scatter off the impurity as if their dynamics are described by the noninteracting Hamiltonian \hat{H}_{qp} . Does this mean that our *a priori* expectations about KWW's quasiparticles were wrong? Could the quasiparticles be bare electrons described by Hewson's \hat{H}_{qp} ? The answer is “no”. \hat{H}_{qp} has a d electron Green's function that is off by a factor z compared to the original Hamiltonian (1). Thus at least the d orbital in \hat{H}_{qp} is an effective, rather than a bare degree of freedom. The fact that low-energy bare electrons scatter elastically does, however, imply the following. If the system is prepared in an eigenstate corresponding to a single quasiparticle on top of the ground state, no particle-hole pairs escape to infinity. Instead, the particle-hole pairs that dress a bare electron to make up a quasiparticle excitation, are confined to a finite region around the impurity. If we write the creation operator for a quasiparticle excitation, as

$$y_d \hat{d}^\dagger + \sum_k y_k \hat{c}_{k\sigma}^\dagger + \text{higher order terms in } \{\hat{d}_\sigma^\dagger, \hat{d}_\sigma, \hat{c}_{k,\sigma}^\dagger, \hat{c}_{k\sigma}\}, \quad (9)$$

then the higher-order terms create particle-hole pairs in the vicinity of the impurity.

B. Aims of this article

In this study we want to shed further light on the structure of the quasiparticles associated with the SIAM. Our aims are (1) to calculate the quasiparticle wave function $y_d, y_k, k = 1, 2, \dots, L$ in Eq. (9) explicitly, (2) to visualize in real space the particle-hole dressed part in the vicinity of the impurity,

described by the higher-order terms in Eq. (9), and (3) see the onset of effects associated with the remnant self-energy $\Sigma^{\text{rem}}(\omega)$ at increased excitation energy. These questions require the development of new methods, as we explain next.

C. Limitations of NRG

For the purposes of numerics, one has to study a system with a finite-dimensional Hilbert space. One possibility is to study a system defined on a regular finite lattice. However, the many-body Hilbert space becomes too large for brute-force methods already at ~ 10 sites. A more sophisticated option is to take an infinite system, and rediscritize it. There is considerable freedom in how to discretize, and particular choices may be better suited to subsequent approximations than others [16]. The general rediscrization procedure works as follows. The energy band is partitioned into intervals \mathcal{E}_k called energy shells. One discrete mode per shell, per channel, is retained, with associated creation operator $\hat{c}_{k\sigma}^\dagger = \int_{\mathcal{E}_k} d\varepsilon \hat{c}_{\varepsilon\sigma}^\dagger / \sqrt{\int_{\mathcal{E}_k} d\varepsilon}$.

Here $\hat{c}_{\varepsilon\sigma}^\dagger$ creates a particle with energy ε and spin σ (in a particular channel). Impurity problems, such as the SIAM, involve local coupling to a point impurity and scattering is therefore s wave, so that only a single channel is involved. Discrete mode k 's energy is taken as the average energy of the interval \mathcal{E}_k . The NRG method, to which we owe many results on fermionic quantum impurity problems, relies on the fact that accurate results can be obtained for low-energy properties, from a cruder description at higher energies. It discretizes the band “logarithmically” so that the density of discrete states scales like $1/|\varepsilon_k - E_F|$. This is done by letting the width of each new interval decrease by a constant factor $1/\Lambda$ compared to the previous one, from the band edges to the Fermi energy. NRG proceeds with a sequence of RG transformations [17]. Step k involves an approximate diagonalization that resolves energies up to shell k . Before the modes in lower-energy shells are included, high-energy states found in the current iteration are discarded, thus avoiding the dimension of the many-body Hilbert space becoming too large to handle. It turns out that the logarithmic discretization ensures accuracy at lower energies being maintained. This accuracy extends to thermodynamic quantities such as specific heat, and impurity spectral quantities such as the local density of states of the d orbital. However, due to the decimation process that keeps the size of the Hilbert space manageable, in practice, only the lowest few single-quasiparticle excitations are found in the end. Furthermore, NRG inherently suffers from poor spatial resolution of correlations in the Fermi sea, because large shells of high-wavelength modes are crudely lumped together into a few discrete modes [11,12]. (Often only two modes are retained to represent the top and bottom quarters of the band, i.e., $\Lambda = 2$.) Our aim is to study the structure of single-quasiparticle modes in terms of bare electron degrees of freedom. This requires us to resolve spatial features all the way down to the Fermi wavelength, which NRG cannot do. Natural orbital methods have recently been shown capable of the required spatial resolution, where ground-state correlations are concerned [15]. In the next subsection we review the application of natural orbital methods to impurity ground-state problems.

D. Covariance matrix and natural orbitals

Given a set of fermionic creation and annihilation operators, associated with an orthonormal single-particle basis, and an arbitrary state $|X\rangle$ in the associated Fock space, the covariance matrix $C(|X\rangle)$ is defined as

$$C_{ij}(|X\rangle) = \langle X | \hat{c}_i^\dagger \hat{c}_j | X \rangle. \quad (10)$$

We will denote the eigenvectors and eigenvalues of the ground-state covariance matrix as follows:

$$\mathbf{x}_\alpha = (x_{1,\alpha}, \dots, x_{L,\alpha})^T, \quad C(|\text{GS}\rangle)\mathbf{x}_\alpha = \lambda_\alpha \mathbf{x}_\alpha. \quad (11)$$

We label eigenvectors and eigenvalues such that $\lambda_1 \geq \lambda_2 \geq \dots \geq \lambda_L$. The eigenvalues of the covariance matrix are independent of the single-particle basis associated to \hat{c}_i . The fermionic creation operators

$$\hat{q}_\alpha^\dagger = \sum_{i=1}^L \hat{c}_i^\dagger x_{i\alpha}, \quad (12)$$

associated to eigenstates of the covariance matrix are known as the natural orbital basis [42]. This basis is independent of the single-particle basis associated to \hat{c}_i . The eigenvalues λ_α are the ground-state occupation probabilities $\langle \text{GS} | \hat{q}_\alpha^\dagger \hat{q}_\alpha | \text{GS} \rangle$ of the natural orbitals. When fermions are held at a finite density, the exclusion principle forces many natural orbitals to have ground-state occupation probabilities near unity. Orbitals that are nearly filled or empty, are inert and cannot participate in many-body correlations. For a given small positive number ϵ , this motivates us to define three sets

$$\begin{aligned} \mathcal{O} &= \{\alpha | \lambda_\alpha > 1 - \epsilon\}, \\ \mathcal{C} &= \{\alpha | \epsilon < \lambda_\alpha < 1 - \epsilon\}, \\ \mathcal{U} &= \{\alpha | \lambda_\alpha < \epsilon\}, \end{aligned} \quad (13)$$

which we call the occupied, correlated, and unoccupied sectors respectively. (Quantum chemists refer to these sets as the inactive, active, and virtual spaces.)

In a quantum impurity problem, the bulk remains noninteracting, and the correlated sector only contains a vanishing fraction of the total number of orbitals in a large system. It was recently realized that for a generic fermionic impurity problem, the number of orbitals in the correlated sector is proportional to $-\ln \epsilon$ at sufficiently small ϵ , with a proportionality constant that remains finite in the thermodynamic limit. As a consequence, the ground state of a generic fermionic impurity model can be approximated as follows, if the natural orbitals are known [40]. Consider a model with N particles. At given ϵ , let $N_{\mathcal{O}}(\epsilon)$ and $N_{\mathcal{C}}(\epsilon)$ be the numbers of orbitals in respectively the occupied and correlated sectors. For sufficiently small ϵ , we can approximate the orbitals in the occupied sector as fully occupied, and those in the unoccupied sector as completely empty, meaning that in the ground state the correlated sector contains $m = N - N_{\mathcal{C}}(\epsilon)$ particles distributed among $N_{\mathcal{C}}(\epsilon)$ orbitals. Let

$$|F\rangle = \hat{q}_{N_{\mathcal{O}}}^\dagger \dots \hat{q}_1^\dagger |0\rangle \quad (14)$$

be the Fermi sea corresponding to the completely filled occupied sector. Given a set of n orbitals $\{\alpha_i\}_n \subset \mathcal{C}$ belonging to

the correlated sector, we define

$$|\{\alpha_i\}_n\rangle = \left(\prod_{\alpha \in \{\alpha_i\}_n} \hat{q}_\alpha^\dagger \right) |F\rangle. \quad (15)$$

Here the prime denotes a fixed ordering of operators (say α decreasing from left to right), to remove ambiguity about the phase of the state. We take as ground-state ansatz, an arbitrary linear combination of N -particle states of the form (15)

$$|\text{GS}\rangle \simeq \sum_{\{\alpha_i\}_m} v_{\{\alpha_i\}_m, \text{GS}} |\{\alpha_i\}_m\rangle. \quad (16)$$

The optimal state is found by minimizing the expectation value of the energy over the coefficients $v_{\{\alpha_i\}_m, \text{GS}}$. Thus it is found that the optimal expansion coefficients $v_{\{\alpha_i\}_m, \text{GS}}$ correspond to the ground-state eigenvector of the effective few-body Hamiltonian

$$[H_{\text{few body}}]_{\{\alpha_i\}_m, \{\beta_i\}_m} = \langle \{\alpha_i\}_m | \hat{H} | \{\beta_i\}_m \rangle. \quad (17)$$

This type of approximation has a long history in quantum chemistry, where it is called the complete active space (CAS) approach [43]. In the context of quantum impurity problems, stronger results regarding accuracy apply than in quantum chemistry, thanks to the proven scaling of the size of the correlated sector with ϵ : The dimension of the effective few-body Hamiltonian is $\binom{N_{\mathcal{C}}(\epsilon)}{m}$, with $m \sim N_{\mathcal{C}}(\epsilon)/2$, which scales exponentially with $N_{\mathcal{C}}$. However, $N_{\mathcal{C}}$ only scales logarithmically with ϵ , and the dimension of the Hamiltonian that has to be diagonalized therefore scales polynomially with $1/\epsilon$. These features of fermionic quantum impurity problems have been exploited to prove that the computational complexity of finding the ground state of a fermionic quantum impurity problem scales quasi-polynomially with the inverse of the required accuracy and polynomially with the system size [39]. What makes the proof nontrivial is the fact that the natural orbitals are defined relative to the ground state, and therefore not known beforehand. In practice, iterative algorithms are found to work well. In these algorithms, a guess for the natural orbitals is recursively improved from the previous iteration's result for the approximate ground state. This is known as the recursive generation of natural orbitals (RGNO) [44]. An early application of the method in a condensed matter context considered a multi-impurity system [48]. Below we find that for the SIAM, the ground-state energy can be determined to an accuracy of 5% of the Kondo temperature, for realistic Kondo temperatures of 1% of the band width, and well-developed correlations (quasiparticle weight $z = 0.2$), using very modest resources, namely a correlated sector consisting of 12 orbitals (six spin up and six spin down), containing six particles (three spin up and three spin down).

It is interesting to note that the covariance matrix of an N -fermion system equals N times the reduced density matrix that is obtained by treating the system as one containing N distinguishable particles that happen to be in an antisymmetric state, and tracing out $N - 1$ of the particles. Natural orbital methods thus use the entanglement spectrum of this single-particle density matrix to assess the extent of correlations. A complementary method to find an optimal noninteracting picture has recently been introduced for bulk interacting systems, where it is more appropriate to obtain a reduced density matrix

by tracing out one of the regions in a spatial bipartitioning of the system under study [50].

E. Discretizations employed

Below, we will study quasiparticles using both NRG and natural orbital methods. As stated above, NRG requires a logarithmic discretization. Natural orbital methods allow more freedom. Here we provide details regarding the different discretizations we will employ. For simplicity, we will work with a continuum model that has a half-bandwidth D throughout, and assume that the continuum model has a flat density of states per unit length so that

$$\Delta = \frac{\pi V^2}{2D}. \quad (18)$$

For a logarithmic discretization, the conduction band is divided into intervals

$$[-D\Lambda^{-k}, -D\Lambda^{-k-1}) \text{ and } (D\Lambda^{-k-1}, D\Lambda^{-k}], \quad (19)$$

with $k = 0, 1, 2, \dots$. The energies of the rediscritized conduction band orbitals are

$$\varepsilon_{k\pm} = \pm \frac{D}{2\Lambda^k} \left(\frac{1}{\Lambda} + 1 \right). \quad (20)$$

After the above discretization, the discrete system still possesses an infinite number of modes. NRG proceeds by turning the diagonal kinetic term into a tri-diagonal form

$$\begin{aligned} \hat{H} = & U \hat{n}_{d\uparrow} \hat{n}_{d\downarrow} + \varepsilon_d (\hat{n}_{d\uparrow} + \hat{n}_{d\downarrow}) + V \sum_{\sigma} (\hat{d}_{\sigma}^{\dagger} \hat{\psi}_{0\sigma} + \hat{\psi}_{0\sigma}^{\dagger} \hat{d}_{\sigma}) \\ & + \sum_{j=0}^{\infty} \sum_{\sigma} t_j (\hat{\psi}_{j\sigma}^{\dagger} \hat{\psi}_{j+1\sigma} + \hat{\psi}_{j+1\sigma}^{\dagger} \hat{\psi}_{j\sigma}), \end{aligned} \quad (21)$$

called the Wilson chain, with the off-diagonal elements $\propto t_j$ describing hopping along the chain. Their explicit form can be looked up in [16]. The first chain site corresponds to the lattice site 0 that is directly coupled to the impurity. Hopping amplitudes decrease like $\Lambda^{-j/2}$ along the chain, with site j associated with energy scale $D\Lambda^{-j/2}$. An infrared cut-off is imposed by truncating the chain after L sites, which yields a finite system, and a smallest-energy scale $\sim D\Lambda^{-L/2}$. We will perform both NRG and natural orbital calculations on the Wilson chain.

The Wilson chain is not suitable for resolving the real-space structure of quasiparticle excitations. We will therefore also use a second, more suitable discretization, in conjunction with natural orbital methods. For this purpose, we take the discrete energies of the finite system to be

$$\varepsilon_k = \frac{k - \Omega - 1}{\Omega} D, \quad L = 2\Omega + 1. \quad (22)$$

To study spatial structure, we interpret the $\hat{c}_{k\sigma}^{\dagger}$ operators associated with these energies as the even modes of a one-dimensional lattice with $4\Omega + 1$ sites, the central site ($j = 0$) of which is side-coupled to the d orbital. We introduce symmetrized position representation operators

$$\hat{\gamma}_{j\sigma} = \sqrt{\frac{1}{2\Omega + 1}} \sum_{k=1}^{2\Omega+1} \cos \left[\frac{\pi j(2k-1)}{4\Omega+2} \right] \hat{c}_{k\sigma}, \quad (23)$$

for $j = 0, \dots, 2\Omega$. (Symmetrization means that $\hat{\gamma}_{j\sigma}$ is one half times the sum of the operators that respectively annihilate an electron on sites j and $-j$. This way we avoid having to introduce creation operators for the odd parity modes that do not couple to the d orbital.) The $\hat{\gamma}_{j\sigma}$ operators obey

$$\{\hat{\gamma}_{j,\sigma}, \hat{\gamma}_{j',\sigma'}^{\dagger}\} = \frac{\delta_{j,j'} \delta_{\sigma,\sigma'}}{(2 - \delta_{j,0})}. \quad (24)$$

Since the infrared-energy cutoff D/Ω scales inversely rather than exponentially with system size, very large systems are required to resolve the emergent infrared physics of quantum impurity models. Natural orbital methods have proved capable of this task, where ground-state properties are concerned.

III. THEORETICAL DEVELOPMENTS

In this section, we present two theoretical developments that we made and which allows us to learn more about the structure of single-quasiparticles in a local Fermi liquid, than was known before. The first is a wave-function picture of local Fermi-liquid theory, applicable to finite systems. This complements Hewson's Green's function picture for infinite systems. It provides us with tools to analyze the structure of single-quasiparticle excitations. The second development is an ansatz for single-quasiparticle excitations in terms of natural orbitals. We will find that results are accurate in a regime where correlations are sufficiently strong to study nontrivial local Fermi liquids, and amenable to discretization on a large regular energy grid.

A. Wave-function picture of local Fermi liquids

Suppose the ground state $|\text{GS}\rangle$, as well as excited states $|\text{p}, n\sigma\rangle$ with a single quasiparticle on top of the ground state, are known to good accuracy. How do we find the (dominant) linear part, cf. Eq. (9) of a quasiparticle operator $\hat{a}_{n\sigma}$ such that

$$|\text{p}, n\sigma\rangle \simeq \hat{a}_{n\sigma}^{\dagger} |\text{GS}\rangle? \quad (25)$$

We can answer this question by setting

$$\hat{a}_{n\sigma} = y_{dn} \hat{d}_{\sigma} + \sum_{k=1}^L y_{kn} \hat{c}_{k\sigma}, \quad |y_{dn}|^2 + \sum_{k=1}^L |y_{kn}|^2 = 1, \quad (26)$$

and maximizing the object function

$$p_n = |\langle \text{GS} | \hat{a}_{n\sigma} | \text{p}, n \rangle|^2, \quad (27)$$

over all unit-length vectors

$$\mathbf{y}_n = (y_{dn}, y_{1n}, \dots, y_{Ln})^T. \quad (28)$$

The optimal solution is found to be

$$y_{dn} = \frac{\langle \text{p}, n | \hat{d}_{\sigma}^{\dagger} | \text{GS} \rangle}{\sqrt{p_n}}, \quad y_{kn} = \frac{\langle \text{p}, n | \hat{c}_{k\sigma}^{\dagger} | \text{GS} \rangle}{\sqrt{p_n}}, \quad (29)$$

The optimal p_n that results is

$$p_n = |\langle \text{GS} | \hat{d}_{\sigma} | \text{p}, n \rangle|^2 + \sum_{k=1}^L |\langle \text{GS} | \hat{c}_{k\sigma} | \text{p}, n \rangle|^2. \quad (30)$$

The quantity p_n is the probability to measure only a single bare electron excitation on top of the ground state when the

state $|p, n\sigma\rangle$ is prepared. The quantity

$$\delta\rho(E) = \sum_n (1 - p_n) \delta(E - E_n), \quad (31)$$

equals the difference in density of single-particle states between a system of bare noninteracting electrons with the same spectrum as the quasiparticles, and the actual system. (Here we do not mean “density of states per unit volume”, but the actual density of states, that diverges in the thermodynamic limit.) The density of states difference remains finite in the thermodynamic limit, and quantifies the extent to which bare electrons are dressed in order to form quasiparticles. It is tempting to use Fermi-liquid Green’s functions, with the remnant self-energy $\Sigma^{\text{rem}}(\omega)$ neglected, to evaluate $\delta\rho$ at low energies in the thermodynamic limit. Since the quasiparticle Green’s function and the actual single-electron Green’s function only differ on the d orbital, one finds $\delta\rho(\omega) = \text{Im}[\tilde{G}_{\sigma\sigma}(\omega) - G_{\sigma\sigma}(\omega)]/\pi$. At the Fermi level, where $\Sigma^{\text{rem}}(\omega) = 0$, this is certainly valid, and gives

$$\delta\rho(0) = \frac{1}{\pi} \left(\frac{1}{\tilde{\Delta}} - \frac{1}{\Delta} \right) = \frac{1}{\pi\Delta} \left(\frac{1}{z} - 1 \right). \quad (32)$$

In a large but finite system, in which the spacing of single-particle levels near the Fermi energy is δE , and p_n varies slowly with n close to the Fermi energy. Equating the right-hand sides of (31) and (32) under these circumstances gives

$$z \simeq \frac{1}{1 + (1 - p_n)\pi\Delta/\delta E}. \quad (33)$$

Thus the wave-function picture of a local Fermi liquid furnishes us with an interpretation of the quasiparticle weight in terms of the bare electron occupation probability.

Above the Fermi level, the reasoning that led to Eq. (32) would predict that $\delta\rho(\omega)$ decreases proportional to $1/(\omega^2 + \tilde{\Delta}^2)$, whereas we expect p_n to decrease and hence $\delta\rho$ to increase as the quality of quasiparticles deteriorates with increasing excitation energy. Below we perform numerics to resolve the behavior of $\delta\rho(\omega)$ at $\omega > 0$.

A mode-resolved measure D_{kn} of how a bare electron is dressed to form the excitation $|p, n\sigma\rangle$ is obtained as follows. Since $|p, n\sigma\rangle = \sqrt{p_n}\hat{a}_{n\sigma}^\dagger|\text{GS}\rangle + |\text{dressing}\rangle$, we set

$$\begin{aligned} D_{kn} &\equiv \langle \text{dressing} | \hat{c}_{k\sigma}^\dagger | \text{GS} \rangle \\ &= \langle p, n\sigma | \hat{c}_{k\sigma}^\dagger | \text{GS} \rangle - \sqrt{p_n} \langle \text{GS} | \hat{a}_{n\sigma} \hat{c}_{k\sigma}^\dagger | \text{GS} \rangle \\ &= \langle p, n\sigma | \hat{c}_{k\sigma}^\dagger | \text{GS} \rangle - \sqrt{p_n} \langle \text{GS} | \{ \hat{a}_{n\sigma}, \hat{c}_{k\sigma}^\dagger \} | \text{GS} \rangle \\ &\quad + \sqrt{p_n} \langle \text{GS} | \hat{c}_{k\sigma}^\dagger \hat{a}_{n\sigma} | \text{GS} \rangle \\ &= \underbrace{\langle p, n\sigma | \hat{c}_{k\sigma}^\dagger | \text{GS} \rangle - \sqrt{p_n} y_{kn}}_{=0} + \sqrt{p_n} \langle \text{GS} | \hat{c}_{k\sigma}^\dagger \hat{a}_{n\sigma} | \text{GS} \rangle \\ &= [\sqrt{p_n} C(|\text{GS}\rangle) y_n]_k, \end{aligned} \quad (34)$$

where we used the definition of y_{kn} [Eq. (29)] twice in the last two lines. This measure equals zero when $|p, n\sigma\rangle$ is associated with a bare electron on top of the ground state (i.e., $p_n = 1$). When the index k refers to wave number, a spatially resolved measure of dressing is obtained by Fourier transforming to real space. Given the arguments presented above, we expect

to see a signal that decays to zero as we move away from the impurity.

Intuitively, we suspect a close link between y_n and the eigenvectors of the type of single-quasiparticle Hamiltonian identified by Hewson. To explore this link, consider the quantities $\langle p, n\sigma | [\hat{H}, \hat{d}_\sigma^\dagger] | \text{GS} \rangle$ and $\langle p, n\sigma | [\hat{H}, \hat{c}_{k\sigma}^\dagger] | \text{GS} \rangle$, where \hat{H} is the particle-hole symmetric SIAM. This leads to the equations

$$\begin{aligned} (E_n - E_{\text{GS}}) \langle p, n\sigma | \hat{c}_{k\sigma}^\dagger | \text{GS} \rangle \\ = \frac{V}{\sqrt{L}} \langle p, n\sigma | \hat{d}_\sigma^\dagger | \text{GS} \rangle + \varepsilon_k \langle p, n | \hat{c}_{k\sigma}^\dagger | \text{GS} \rangle, \end{aligned} \quad (35)$$

and

$$\begin{aligned} (E_n - E_{\text{GS}}) \langle p, n\sigma | \hat{d}_\sigma^\dagger | \text{GS} \rangle \\ = U \langle p, n\sigma | (\hat{n}_{d-\sigma} - 1/2) \hat{d}_\sigma^\dagger | \text{GS} \rangle + \frac{V}{\sqrt{L}} \sum_{k=1}^L \langle p, n\sigma | \hat{c}_{k\sigma}^\dagger | \text{GS} \rangle. \end{aligned} \quad (36)$$

If

$$\frac{U \langle p, n\sigma | (\hat{n}_{d-\sigma} - 1/2) \hat{d}_\sigma^\dagger | \text{GS} \rangle}{\frac{V}{\sqrt{L}} \sum_{k=1}^L \langle p, n\sigma | \hat{c}_{k\sigma}^\dagger | \text{GS} \rangle} \equiv (1 - z) \quad (37)$$

does not vary much as a function of n , we can employ it as a definition of the quasiparticle weight z . That the above-defined z is approximately independent of n for low-energy states can be made plausible by noting that $(\hat{n}_{d-\sigma} - 1/2)\hat{d}_\sigma^\dagger$ and $\sum_{k=1}^L \hat{c}_{k\sigma}^\dagger/\sqrt{L}$ probe the system locally at one end, while $n \rightarrow n+1$ affects the phase difference between amplitudes on adjacent sites by an amount $\sim 1/L \ll 1$ only. Note that via (36) and (37) is equivalent to

$$z = \frac{(E_n - E_{\text{GS}}) \langle p, n\sigma | \hat{d}_\sigma^\dagger | \text{GS} \rangle}{\frac{V}{\sqrt{L}} \sum_{k=1}^L \langle p, n\sigma | \hat{c}_{k\sigma}^\dagger | \text{GS} \rangle}. \quad (38)$$

We substitute (37) into (36) and define

$$\psi_{dn} = \frac{\langle p, n\sigma | \hat{d}_\sigma^\dagger | \text{GS} \rangle}{\sqrt{z}}, \quad \psi_{kn} = \langle p, n\sigma | \hat{c}_{k\sigma}^\dagger | \text{GS} \rangle, \quad (39)$$

and $\tilde{V} = \sqrt{z}V$, to obtain the effective single-quasiparticle Schrödinger equation

$$\begin{aligned} (E_n - E_{\text{GS}}) \psi_{kn} &= \frac{\tilde{V}}{\sqrt{L}} \psi_{dn} + \varepsilon_k \psi_{kn}, \\ (E_n - E_{\text{GS}}) \psi_{dn} &= \frac{\tilde{V}}{\sqrt{L}} \sum_{k=1}^L \psi_{kn}, \end{aligned} \quad (40)$$

associated with a noninteracting SIAM ($U = 0$) and a renormalized hybridization $\tilde{\Delta} = z\Delta$. This is precisely the form identified by Hewson, and implies that $\psi_{dn} = \sqrt{p_n/z} y_{dn}$, $\psi_{kn} = \sqrt{p_n} y_{kn}$.

B. Ansatz

Next, we explain our approach to generalizing natural orbital methods to excited states. We consider $N \pm 1$ particle excited states that are obtained by adding or removing a particle from the noninteracting system, and adiabatically switching on the interaction. If the low-energy physics is

that of a local Fermi liquid, these excitations will be single-quasiparticle- or -hole-like in nature.

Based on the notion that the natural orbital basis minimizes the Hamiltonian's ability to generate particle-hole pairs, we make the following ansatz for excited states consisting of one particle on top of the ground state:

$$|p, k\rangle_1 = \sum_{\alpha \in \mathcal{U}} u_{\alpha,k} \hat{q}_\alpha^\dagger |\text{GS}\rangle + \sum_{\{\alpha_i\}_{m+1}} v_{\{\alpha_i\}_{m+1},k} |\{\alpha_i\}_{m+1}\rangle. \quad (41)$$

The first term represents a single uncorrelated particle in what was the unoccupied sector for the ground state. The second term represents a particle added to the correlated sector, and allowed to form an arbitrary correlated state with the m particles already present. This amounts to assuming that

(1) adding a particle leaves the occupied sector undisturbed,

(2) there is at most one particle in the unoccupied sector,

(3) and if the added particle ends up in the unoccupied sector, the particles in the correlated sector are not disturbed from the way they were configured in the ground state.

[Of these assumptions, the last one (3) seems the most arbitrary. In the Appendix we therefore investigate the consequences of not making this assumption. The conclusion is that assumption (3) does in fact apply in the local Fermi-liquid regime.] We find the coefficients $u_{\alpha,k}$ and $v_{\{\alpha_i\}_{m+1},k}$ variationally. Formally, we first find the lowest-energy state of this form, then we vary orthogonal to the lowest-energy state, to get the second lowest-energy state and so on. Luckily, one does not ever explicitly have to parametrize the space orthogonal to the states found already: It is easy to show that the coefficients of the states obtained in the procedure are simply the eigenvectors of the effective Hamiltonian

$$H_p = \begin{pmatrix} H_{\mathcal{U}\mathcal{U}} & H_{\mathcal{U}\mathcal{C}} \\ H_{\mathcal{U}\mathcal{C}}^\dagger & H_{\mathcal{C}\mathcal{C}} \end{pmatrix}, \quad (42)$$

consisting of the blocks

$$\begin{aligned} [H_{\mathcal{U}\mathcal{U}}]_{\alpha,\beta} &= \langle \text{GS} | \hat{q}_\alpha \hat{H} \hat{q}_\beta^\dagger | \text{GS} \rangle, \\ [H_{\mathcal{U}\mathcal{C}}]_{\alpha, \{\beta_i\}_{m+1}} &= \langle \text{GS} | \hat{q}_\alpha \hat{H} | \{\beta_i\}_{m+1} \rangle, \\ [H_{\mathcal{C}\mathcal{C}}]_{\{\alpha_i\}_{m+1}, \{\beta_i\}_{m+1}} &= \langle \{\alpha_i\}_{m+1} | \hat{H} | \{\beta_i\}_{m+1} \rangle. \end{aligned} \quad (43)$$

The dimension of this Hamiltonian is $N_{\mathcal{U}} + \binom{N_{\mathcal{C}}}{m+1}$, where $N_{\mathcal{U}}$ is the number of orbitals in the unoccupied sector. Similar to the ansatz for particle-like excitations, we make an ansatz for hole-like excitations.

$$|h, k\rangle_1 = \sum_{\alpha \in \mathcal{O}} u_{\alpha,k} \hat{q}_\alpha |\text{GS}\rangle + \sum_{\{\alpha_i\}_{m-1}} v_{\{\alpha_i\}_{m-1},k} |\{\alpha_i\}_{m-1}\rangle. \quad (44)$$

We note that variational trial states with limited numbers of particles in the unoccupied sector and holes in the occupied sector have been employed before in the context of quantum impurity problems [47,51], but as far as we know, not to calculate excited quasiparticle states.

To gauge the accuracy of the ansatz, we benchmarked it against NRG results. Details can be found in the Appendix. This allowed us to identify SIAM parameters that produce a well-developed Kondo regime, and in which the ansatz gives accurate results at an affordable computational cost.

IV. NUMERICAL RESULTS

We now present numerical results that we obtained by applying the tools developed in Sec. III A to eigenstates of the SIAM that comprise a single quasiparticle on top of the ground state. We obtained the latter by means of NRG, or more approximately, using the ansatz (41).

A. The bare electron occupation probability p_n and the DOS difference $\delta\rho$

We have performed numerical investigations on the particle-hole symmetric SIAM using NRG and the ansatz (41). In this subsection we show results for $\Delta = 0.09D$ and $U = 0.6D$, which correspond to $T_K = 0.013D$. In Fig. 1 we present results for the bare electron occupation probability p_n (27) and the difference in single-particle DOS (31) between the quasiparticle Hamiltonian (40) and the actual system. We present NRG results for different Wilson chain lengths L (infrared-energy cut-offs) for the same SIAM parameters. For each L , NRG could find the lowest n_L single-particle excitations, with n_L between 2 and 4. (Higher excited single-quasiparticle excitations get decimated during the renormalization flow.) In order to access higher-energy single-quasiparticle excitations, we employed the ansatz (41) on the same Wilson chain Hamiltonian as NRG. We used a correlated sector with six spin up and six spin down orbitals, that is half-filled for the ground state. At each L we see that there is a slight decrease in p_n going from the lowest single-quasiparticle excitation to the second lowest. There is a steeper decrease of p_n going from the second to the third, third to fourth excitation, and so on. The fact that the lowest single-quasiparticle excitation behaves differently than the rest has to do with the energy discretization employed by NRG, in which the inverse of the level spacing between single-particle states of the Wilson chain has a similar behavior. At fixed L , $1 - p_n$ is proportional to E_n , for $n = 2, 3, 4$, with an L -independent proportionality constant. For the lowest single-quasiparticle state ($n = 1$) at different L , we also find $1 - p_1 \propto E_1$. We see good agreement between NRG and the ansatz. When L is varied, the $1 - p_n \propto E_n$ behaviour breaks down when the infrared cut-off scale is $\sim 0.1T_K$. The ansatz accurately captures the $1 - p_n \propto E_n$ behavior, but is less accurate at $L \lesssim 23$ when the infrared cut-off scale encroaches on T_K .

We obtain the DOS difference $\delta\rho$ by multiplying $1 - p_n$ by the density of single-particle energies of the Wilson chain $= 1/\ln(\Lambda)E_n$, cf. Eq. (31). To avoid having to deal with the irregularity of the level spacing at the lowest single-quasiparticle state, we exclude it from the presented results in the right panel of Fig. 1. At $E_n \ll T_K$, $\delta\rho$ is constant. NRG results show that $\delta\rho$ increases above the low-energy plateau, if the system's infrared cut-off energy scale is larger than $0.1T_K$. The ansatz does not reproduce this behavior of systems in which the infrared scale encroaches on the Kondo scale. In other words, when the Fermi-liquid picture starts breaking down, the accuracy of the ansatz deteriorates. However, the ansatz still yields the qualitatively correct behavior that $\delta\rho$ rapidly increases for excitations around the Kondo scale.

NRG is sufficient to show that $\delta\rho$ increases above the low-energy plateau, if the system's infrared cut-off energy

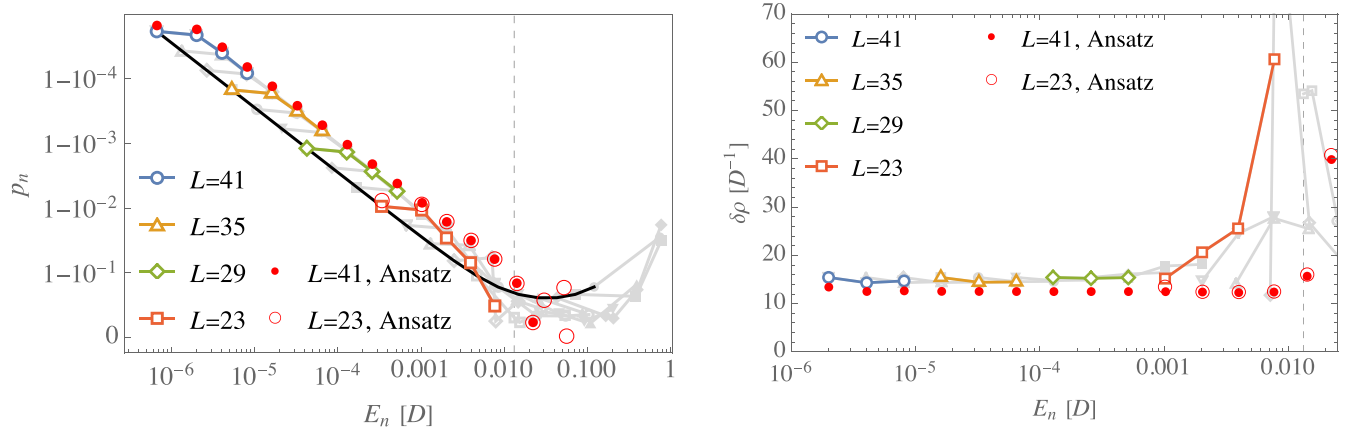


FIG. 1. (Left) The probability p_n (27) to detect only a bare electron above the ground state for the symmetric SIAM with $\Delta = 0.09D$ and $U = 0.6D$. (Right) The difference $\delta\rho$ [Eq. (31)] between the density of states of the single-quasiparticle Hamiltonian (40) and the single-particle density of states of the actual Hamiltonian, calculated from the same data. Results are shown for all states with $p_n > 0.5$. The grey data represent NRG results for Wilson chains of lengths of $L = 2\Omega + 1$ with $\Omega = 1, 8, \dots, 20$ and $\Lambda = 2$. The black solid curve in the left panel connects the data points corresponding to the lowest-energy states with one particle on top of the ground state, at different L . In the right panel, the states connected by this black line were omitted. The dashed vertical line indicates the Kondo temperature (3). NRG results at representative L are highlighted as indicated in the legend. Results obtained with the ansatz, on the same Wilson chain as used in NRG, are plotted with the symbols indicated in the legend.

scale is larger than $0.1T_K$. However, the ansatz is required to study single-quasiparticle excitations close to T_K when the system's infrared cut-off scale is much lower than T_K . The ansatz indicates that in this case, $\delta\rho$ remains constant up to nearly T_K , after which it increases. An increase of $\delta\rho$, rather than a decrease, validates the intuition articulated in Sec. III, that $\delta\rho$ reveals deviations from perfect Fermi-liquid behavior when the system is probed at energies approaching T_K .

In Sec. III, we predicted [Eq. (32)] that the value of $\delta\rho$ on the low-energy plateau should be $(1/z - 1)/\pi\Delta$ where z is the quasiparticle weight. We test this prediction as follows. Using NRG, we calculate the plateau value of $\delta\rho$ for different U and Δ . For each calculation, we also determine z by fitting the low-energy spectrum to that of a noninteracting SIAM ($U = 0$), with renormalized $\tilde{V} = \sqrt{z}V$ [Eq. (40)]. The results of this analysis are shown in Fig. 2. We see very good agreement between NRG results and our prediction. This confirms the validity of the interpretation given to the quasiparticle weight z within the wave-function picture of local Fermi-liquid theory, namely that it is connected to the bare electron occupation probability via (33).

B. Quasiparticle weight and wave function

In Sec. III, we made a connection (39) between the matrix elements $\langle p, n\sigma | \hat{d}_\sigma^\dagger | \text{GS} \rangle$ and $\langle p, n\sigma | \hat{c}_{k\sigma}^\dagger | \text{GS} \rangle$ on the one hand, and eigenvectors of a single-quasiparticle Hamiltonian (40) on the other. This rests on the assumption that a quasiparticle weight z , approximately independent of excitation energy, can be defined through either Eq. (37) or equivalently Eq. (38). In Fig. 3 we validate this assumption. In the left panel, we compare several quantities calculated with NRG, for the particle-hole symmetric SIAM. The dashed line was obtained by fitting the spectrum of single-quasiparticle Hamiltonian (40) for given quasiparticle weight z , to the low-energy spectrum obtained by NRG. (This is the same procedure as was

followed to obtain z in Fig. 2.) The symbols represent the two equivalent expressions (37) and (38) evaluated for every low-energy eigenstate found by NRG, that has $p_n > 0.5$. Results for Wilson chains of different lengths L are shown together. There is a clear agreement between the conventional definition of the quasiparticle weight, represented by the dashed line, and the symbols representing Eqs. (37) and (38). However, there also appear some outliers. Given any exact eigenstate, the quantity represented by the dots should equal the quantity represented by the disks, regardless of whether they equal the energy-independent quasiparticle weight. At the lowest energies (corresponding to the longest Wilson chains) the dots and the open disks do not lie on top of each other. This indicates that these low-energy deviations are an artefact due to the inherent numerical instability of calculating matrix

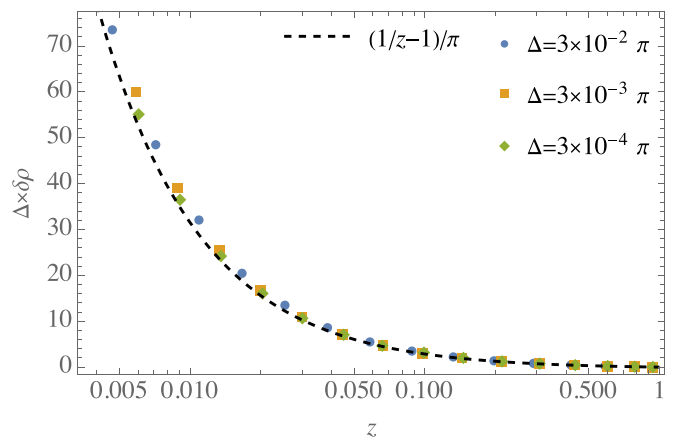


FIG. 2. Hybridization Δ times the density of states difference $\delta\rho$ [Eq. (31)], for different U and three values of Δ , vs the corresponding quasiparticle weight z . A dashed line indicates the estimate [Eq. (32)].

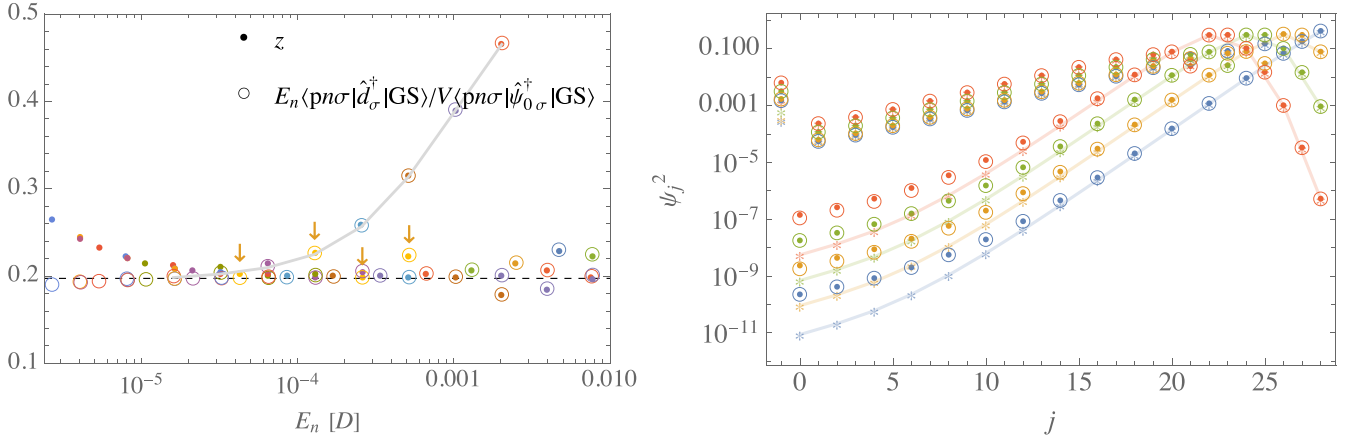


FIG. 3. (Left) The quasi-particle weight z , for the symmetric SIAM with $\Delta = 0.09D$ and $U = 0.6D$. Results were obtained with NRG on Wilson chains of lengths of $L = 2\Omega + 1$ with $\Omega = 7, 8, \dots, 20$ and $\Lambda = 2$. Different colors represent different L . Each plot marker represents a single-quasiparticle excitation. Dots represent the estimate (37) while open disks represent the estimate (38). The dashed line was obtained from $z = \tilde{V}^2/V^2$, where \tilde{V} was determined by fitting the spectrum of the quasiparticle Hamiltonian (40) to the single-particle spectrum found in NRG, at $L = 29$. (Right) Square of the quasiparticle wave functions ψ_j , with unit-normalization, for the symmetric SIAM with $\Delta = 0.09D$ and $U = 0.6D$ on a Wilson chain of length of $L = 29$. (Here $j = -1$ refers to the d orbital.) The lowest four single-quasiparticle wave functions are shown. The dots were calculated with NRG. The open circles represent the wave functions calculated using the single-quasiparticle Hamiltonian (40). The quasiparticle weight represented by the dashed line in the left panel was employed. The stars show the single-particle wave functions of the noninteracting $\Delta = 0.09D$, $U = 0$ problem, for comparison.

elements of irrelevant operators near the infrared fixed point. Another branch of outliers are indicated by a solid grey curve. Tracing this curve from right to left, it eventually merges with the correct value of z . We have identified that this branch is associated with hybridization on the Wilson chain between the second single-quasiparticle eigenstate and the lowest excited state containing two quasiparticles and one quasi-hole. During the renormalization flow, these two many-body levels approach each other. Initially there is some level repulsion and associated hybridization. However, eventually (for sufficiently long Wilson chains) the two become degenerate, so that a well-developed single-quasiparticle excitation can be distinguished. This is the point where the branch merges with the plateau indicated by the dashed line. This branch therefore does not represent a failure of the theory developed in Sec. III, but rather a genuine interaction between quasiparticles at intermediate energies. In other words, if the finite Wilson chain with $L \leq 31$ could be weakly connected to leads, the considered outliers would represent a scattering resonance, due to an accidental degeneracy, in which an incoming electron really does scatter into two electrons and a hole.

In the right panel of Fig. 3, we plot the square of $\psi_{dn} = \langle p, n\sigma | \hat{d}_\sigma^\dagger | \text{GS} \rangle / \sqrt{z}$ and $\psi_{jn} = \langle p, n\sigma | \hat{c}_{j\sigma}^\dagger | \text{GS} \rangle$ (39) with the matrix elements calculated by means of NRG, and $z = 0.197$ as indicated by the dashed line in the left panel. Here j is the site-index along the Wilson chain, and $j = -1$ corresponds to the d orbital. (We normalized ψ_n to unity.) We compare this to the single-particle eigenvectors of the quasiparticle Hamiltonian (40), at the same quasiparticle weight. Results are shown for the four lowest quasiparticle states of the $L = 29$ chain that are indicated by arrows in the left panel. For comparison, we also show the single-particle wave functions of the noninteracting ($U = 0$, $z = 1$) chain, with the same bare hybridization $\Delta = 0.09D$. We see

near perfect coincidence between the NRG results and the single-quasiparticle wave functions at $z = 0.197$. We also note that amplitudes on low-energy shells (large j) are nearly independent of z . The quasiparticle weight (or renormalized hybridization) only affects the very small amplitudes on energy shells $j = 0, 2, \dots$ up to the shell at the Kondo scale. This is a manifestation of the fact that the hybridization term in the Hamiltonian represents an irrelevant perturbation around the infrared fixed point (albeit a leading one).

C. Mode-resolved dressing

Next we present results for the mode-resolved dressing measure D_{jn} , cf. Eq. (34). We work on the Wilson chain, in the site basis j , i.e., we resolve dressing per energy shell. We have already investigated the total amount of dressing of a single-quasiparticle state, by calculating p_n . Here we therefore normalize each D_{jn} such that $\text{Max}\{D_{jn} | j = d, 0, 1, \dots, L-1\} = 1$. In Fig. 4, we present NRG results for $|D_{jn}|^2$, for the lowest four single-quasiparticle states $n = 1, 2, 3, 4$, for Wilson chains of different length. For chains long enough that the infrared cut-off scale is less than $\sim 0.1T_K$, we see that D_{jn} has the same shape for $n = 1, 2, 3, 4$, and for different L . This is a nontrivial observation, since the associated y_n , $n = 1, 2, 3, 4$ used to calculate D_{jn} are clearly distinct. It means that low-energy quasiparticles associated with different single-particle orbitals are dressed in the same form. We find that D_{jn} is peaked at an energy shell above T_K . This reflects the fact that one has to probe the system at ultraviolet scales to distinguish a quasiparticle from a bare electron. Regarding L dependence, we see that D_{jn} starts changing when the Wilson chain is so short that the tail of D_{jn} extends to the lowest-energy shell. This behavior confirms that the proposed measure really does give the correct mode-resolved picture: As the length L of the Wilson chain is decreased, the nature of quasiparticles

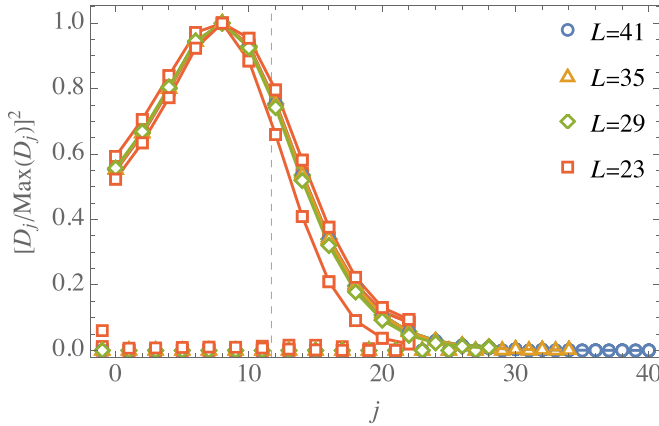


FIG. 4. NRG results for the dressing D_j , Eq. (34) normalized so that $\max(D_j) = 1$, for the symmetric SIAM with $\Delta = 0.09D$ and $U = 0.6D$. Results were obtained with NRG on Wilson chains of lengths as indicated in the legend and $\Lambda = 2$. At each length, the lowest four single particle states are plotted. They lie on top of each other, except for $L = 23$. The dashed vertical line indicates the position of Kondo temperature (3) relative to the energy shells j of the Wilson chain.

starts changing when the low-energy dressing cannot fit on the Wilson chain any more.

We now return to the low-energy behavior of (normalized) D_{jn} . In the left panel of Fig. 5, we show results for the lowest eigenstate with one quasiparticle on top of the ground state ($n = 1$) for different combinations of Δ and U , all chosen such that $T_K \ll D$. We see that the general shape is rather similar for vastly different parameters. (Of course, if we did not normalize, the overall amplitude would depend strongly on T_K .) In the right panel, we replot the same data in log scale on the vertical axis, and shifted horizontally to line up the maxima of the different data sets at $j = 0$. At small j (i.e., in the ultraviolet) we see exponential behavior that depends on Δ , but not on U . In the infrared (large j), we obtain univer-

sal behavior $D_{jn} \sim e^{-\alpha j}$ independent of Δ or U . For $\Lambda = 2$ we find $\alpha \sim 0.16$. Translating from shell index to energy and then to momentum, this implies $D_{jn} \sim k^{2\alpha/\ln(\Lambda)}$, where k measures momentum relative to the Fermi momentum. We repeated the calculations at $\Lambda = 3$ (not shown) and find results consistent with $\alpha/\ln(\Lambda) \simeq 0.23$ independent with Λ . This suggests power-law decay of the dressing at sufficiently large distances with an exponent $1 + 2\alpha/\ln(\Lambda) = 1.46$ independent of Kondo temperature. To obtain such a nontrivial power law that does not depend on Kondo temperature seems rather suspicious. We believe that it is an artefact of logarithmic discretization, which is known to prevent the accurate resolution of other real space correlations, such as the Kondo cloud.

D. Real-space quasiparticle structure

To access the properties of single-quasiparticle excitations in real space, we therefore proceed to study the structure of single-quasiparticle states on a regular energy grid (22) of $L = 2\Omega + 1$ levels with $\Omega = 2400$, using natural orbital methods. We take $\Delta = 0.09$ as above, and work at the relatively weak interaction strength $U = 0.2D$. According to NRG, the quasiparticle weight $z = 0.77$ and the Kondo temperature is $0.064D$. We have benchmarked the ansatz at this point in parameter space by calculating the Kondo resonance of the local density of states of the d orbital. We find that the ansatz is accurate for excitation energies up to $\sim 0.3T_K$. (See Appendix. For fixed size of the correlated sector, the ansatz on the large linear grid seems to be somewhat less accurate than on the logarithmic grid. On the linear grid and with $U = 0.6$ for instance, errors in the 10% range are found for quantities such as the quasiparticle weight. This is why we chose to work with $U = 0.2D$ here.)

Previously, in the right panel of Fig. 1, we confirmed that matrix elements $\langle p, n\sigma | \hat{d}_\sigma^\dagger | \text{GS} \rangle / \sqrt{z}$ and $\langle p, n\sigma | \hat{c}_{k\sigma}^\dagger | \text{GS} \rangle$ are eigenvectors of the single-quasiparticle Hamiltonian (40) for the Wilson chain. Now we perform the equivalent analysis for

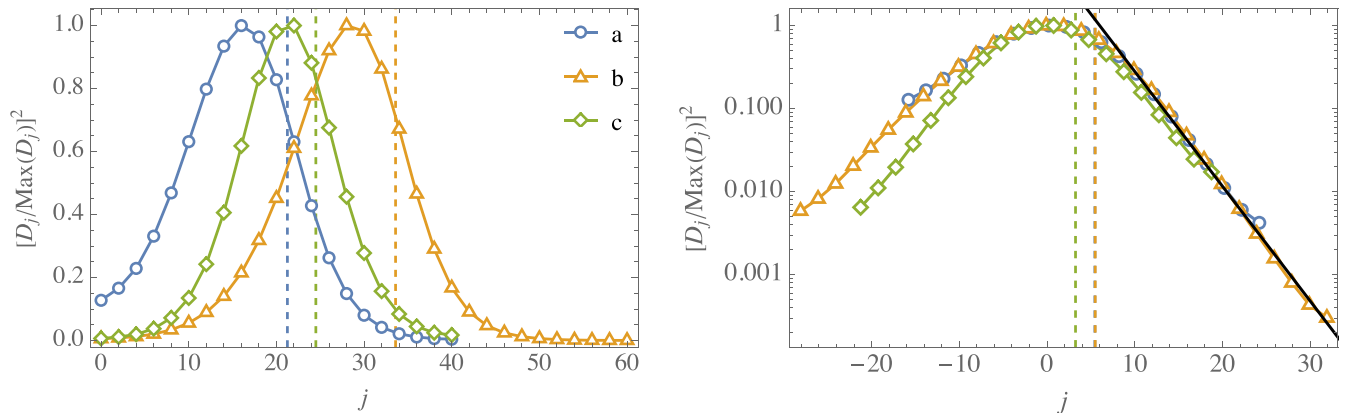


FIG. 5. (Left) Comparison of NRG results for the dressing D_j , Eq. (34) normalized so that $\max(D_j) = 1$, for the symmetric SIAM for different Δ and U . The three data sets are for (a) $\Delta = 0.09D$, $U = 1.4D$, (b) $\Delta = 0.09D$, $U = 2.4D$, and (c) $\Delta = 0.0009D$, $U = 0.006D$. The corresponding Kondo temperatures T_K are respectively $4.7 \times 10^{-4}D$, $6.6 \times 10^{-6}D$, and $1.5 \times 10^{-4}D$. The lowest state with a single quasiparticle on top of the ground state is plotted in each case. Results were obtained with NRG on Wilson chains with $\Lambda = 2$. The dashed vertical lines indicate the positions of Kondo temperatures (3) relative to the energy shells j of the Wilson chain. (Right) Same data as left panel, but plotted in log scale on the vertical axis, and shifted horizontally so the maxima occur at zero. The black line is proportional to $e^{-0.32j}$.

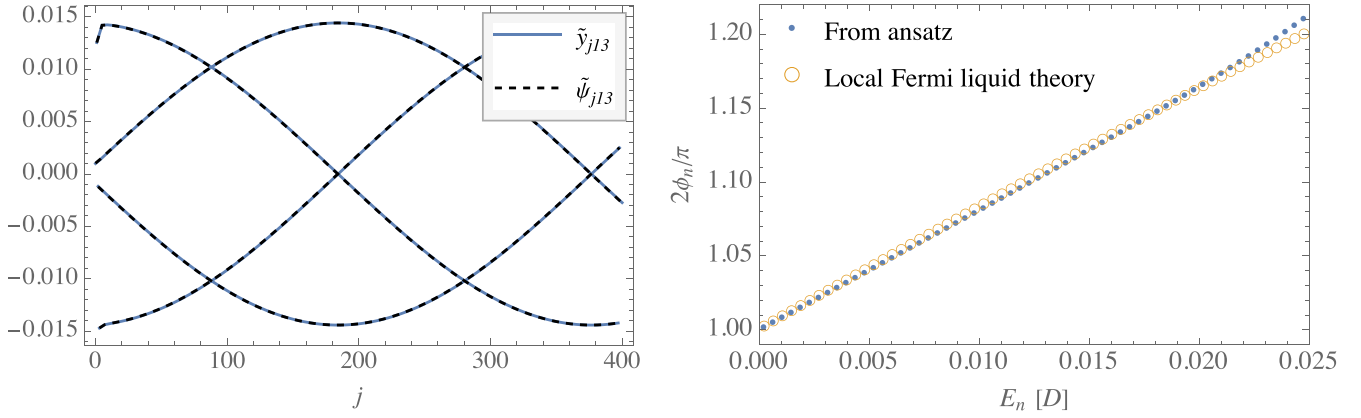


FIG. 6. (Left) A representative position space quasiparticle wave function (the 12th excited single quasiparticle state) for the symmetric SIAM with $\Delta = 0.09D$ and $U = 0.2D$ calculated on a regular 1D lattice of 9601 sites, with the d orbital coupled to the central site ($j = 0$). The solid curves represent the result obtained with the ansatz, while the dashed curves represent the corresponding eigenvector of the single-quasiparticle Hamiltonian (40), with the quasiparticle weight estimated as indicated by the dashed line in the left panel of Fig. 3. Each curve was obtained by connecting amplitudes on every fourth site, starting at sites 0, 1, 2, or 3. (Right) The phase shift. Results extracted from the ansatz, using Eq. (46) are indicated by dots. The open disks were obtained from the single-quasiparticle Hamiltonian on the regular 1D lattice (40), with the renormalized hybridization \tilde{V} inferred from NRG calculations similar to those in Sec. IV B.

the large regular energy grid, to establish whether the equality holds at single real-space lattice site resolution.

In the left panel of Fig. 6, we plot $y_{kn} = \langle p, n\sigma | \hat{c}_{k\sigma}^\dagger | \text{GS} \rangle$, Fourier transformed to real space, i.e.,

$$\tilde{y}_{jn} = \frac{1}{\sqrt{2\Omega+1}} \sum_{k=1}^{2\Omega+1} \cos\left[\frac{\pi j(2k-1)}{4\Omega+2}\right] y_{kn}. \quad (45)$$

We can check this against the predictions of local Fermi-liquid theory as follows. First we extract the renormalized \tilde{V} by fitting the low-energy NRG spectrum to the Wilson chain version of the single-quasiparticle Hamiltonian (40). Using this \tilde{V} , we compute the eigenvectors ψ_n of the single-quasiparticle Hamiltonian (40) discretized on the regular energy lattice. We Fourier transform and suitably normalize the bulk amplitudes to obtain $\tilde{\psi}_{jn}$. This is compared to \tilde{y}_{jn} . As a representative example, we look at the 12th excited single-quasiparticle state (i.e., $n = 13$), and see near-perfect agreement.

Except for the first few sites, \tilde{y}_{jn} is a shifted sinusoidal wave

$$\tilde{y}_{jn} \simeq A_n \cos(|j|k_n - \phi_n). \quad (46)$$

We extract the phase shift ϕ_n by fitting (46) to \tilde{y}_{jn} , and remembering that the boundary condition $\tilde{y}_{2\Omega+2,n} = 0$ imposes the quantization

$$k_n = k_F + \frac{\pi n - \phi_n}{2\Omega + 1}, \quad (47)$$

of the wave number. We can compare this to the predictions of local Fermi-liquid theory by similarly extracting the phase shift of $\tilde{\psi}_{jn}$. In the right panel of Fig. 6, we see that the two estimates agree very well up to $E_n = 0.02D \sim 0.3T_K$. We conclude that indeed the matrix elements y_{dn}/\sqrt{z} and \tilde{y}_{jn} represent a real-space eigenvector of the single-quasiparticle Hamiltonian (40).

If a noninteracting quasiparticle picture holds, we should equivalently be able to extract the phase shift from the quantization of the wave number and the dispersion relation as

follows:

$$E_n = \frac{2\Omega + 1}{\pi\Omega} (k_n - k_F) \Rightarrow \phi_n = \pi \left(n - \frac{\Omega E_n}{D} \right). \quad (48)$$

We have checked that applying this method to results obtained with the ansatz gives the same result as the dots in the right panel of Fig. 6.

Finally, we study the dressing profile in real space. That is, we compute D_{kn} for the system discretized on a regular energy grid, and Fourier transform as Eq. (45) to obtain the site-resolved dressing \tilde{D}_{jn} . The results presented in the left panel of Fig. 5, suggests that \tilde{D}_{jn} is a good measure of how different from a bare electron the quasiparticle excitation looks on real-space lattice site j . In Fig. 7, we show results at $U = 0.2D$, which are quantitatively accurate, and results at $U = 0.6D$, that may contain small but non-negligible errors. We compare the lowest eigenstate with one quasiparticle on top of the ground state in each case, for which the ansatz should give more accurate results than for higher excited states. We therefore think that the error in the $U = 0.6D$ results are smaller than the 10% errors observed for quantities such as the quasiparticle weight, that tests the ansatz at higher excited states. As expected we see that the dressing decays as we move away from the impurity, and that increasing U , which decreases T_K , leads to more significant dressing. At large distances, the dressing profile seems to satisfy a power law $\sim j^{-b}$ with b discernibly different from 1. For $U = 0.2D$ we find $b = 0.97$, while for $U = 0.6D$ we find $b = 0.93$. The decrease of the exponent at larger U is consistent with the expectation that the particle-hole pairs that dress the bare electron are less confined, the lower the Kondo temperature, but it has to be kept in mind that the $U = 0.6D$ results are less accurate than the $U = 0.2D$ results. We are therefore less confident about the exact value of the exponent at $U = 0.6D$ than at $U = 0.2D$. Nonetheless, evidence of a nontrivial power law is clear, and the fact that the decay is slower for stronger interactions is more plausible than the interaction strength independent

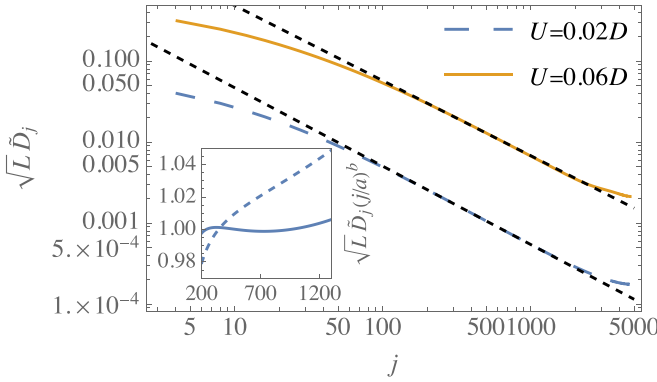


FIG. 7. The dressing measure D_j Fourier transformed to real space as in Eq. (45), for the symmetric SIAM calculated on a regular 1D lattice of 9601 sites, with the d orbital coupled to the central site ($j = 0$) at $\Delta = 0.09D$ and two values of U . The curves are envelopes to the actual data, and were obtained by plotting the result on each fourth site, $j = 4l$, $l = 0, 1, \dots$. In each case the lowest single-quasiparticle state as obtained by the ansatz, was used to calculate D_j . The dashed lines represent a fit to a power law $(a/j)^b$. For $U = 0.2$ we found a best fit $b = 0.97$ and for $U = 0.6$ we found $b = 0.93$. (Inset) The solid curve represents $\sqrt{L}\tilde{D}_j \times (j/a)^b$ for $U = 0.2D$, with $a = 0.43$ and $b = 0.97$ determined in the main panel by fitting $(a/j)^j$ to $\sqrt{L}\tilde{D}_j$. The dashed curve represents $\sqrt{L}\tilde{D}_j \times (j/a)$ for $U = 0.2D$, with $a = 0.53$ determined by fitting a/j to $\sqrt{L}\tilde{D}_j$. From this we deduce that the data is sufficient to reveal that the power law is $\tilde{D}_j \sim j^{-0.97}$ rather than $\tilde{D}_j \sim j^{-1}$ at $U = 0.2D$.

prediction obtained employing a logarithmic discretization of the conduction band.

V. SUMMARY AND CONCLUSIONS

There are two distinct single-particle-like structures associated with dynamic fermionic quantum impurity problems. There are the quasiparticles that provide a local Fermi-liquid description of low-energy excitations in terms of independent *effective* degrees of freedom. Then there is also the natural orbital basis, associated with the *bare* electronic degrees of freedom, which is known to provide an economical description of ground-state correlations. The study presented here was inspired by the question: “Can a synergy of these two pictures shed light on how bare electrons are dressed to form the quasiparticle excitations of a local Fermi liquid?”. We succeeded in establishing the following. The quasiparticle weight z , and the effective quasiparticle Hamiltonian

$$\hat{H}_{\text{qp}} = \sqrt{z}V \sum_{\sigma} (\hat{d}_{\sigma}^{\dagger} \hat{\psi}_{0\sigma} + \hat{\psi}_{0\sigma}^{\dagger} \hat{d}_{\sigma}) + \sum_{k=1}^L \sum_{\sigma} \varepsilon_k \hat{c}_{k\sigma}^{\dagger} \hat{c}_{k\sigma}, \quad (49)$$

of the particle-hole symmetric single impurity Anderson model have meaning not only in the infinite system, where they determine the scattering matrix of electrons at low energy, but also in the large finite system. If $|p, n\sigma\rangle$ is a low-energy single-quasiparticle excited state of the SIAM, then to a good approximation $\psi_{dn} = \langle p, n\sigma | \hat{d}_{\sigma}^{\dagger} | \text{GS} \rangle / \sqrt{z}$ and $\psi_{kn} = \langle p, n\sigma | \hat{c}_{k\sigma}^{\dagger} | \text{GS} \rangle$ solve the single-particle Schrödinger equation (40) associated with Eq. (49). Furthermore, if we define $y_{dn} = \sqrt{z/p_n} \psi_{dn}$ and $y_{kn} = \psi_{kn} / \sqrt{p_n}$ with p_n such that

$(y_{dn}, y_{1n}, \dots, y_{Ln})$ is normalized to unity, then $\hat{a}_{n\sigma}^{\dagger} = y_{dn} \hat{d}_{\sigma}^{\dagger} + \sum_{k=1}^L y_{kn} \hat{c}_{k\sigma}^{\dagger}$ represents the best bare electron approximation to the quasiparticle associated with $|p, n\sigma\rangle$. We call p_n the bare electron occupation probability because it is the occupation probability of the $\hat{a}_{n\sigma}$ orbital when the system is in state $|p, n\sigma\rangle$. In a system where the single-quasiparticle level spacing is δE in the vicinity of excitation $|p, n\sigma\rangle$, at low energies, p_n is nearly independent of energy and related to the quasiparticle weight z by $z = 1/[1 + (1 - p_n)\pi\Delta/\delta E]$. We define the dressing of the bare electron as $|\text{dressing}\rangle = |p, n\sigma\rangle - \sqrt{p_n} \hat{a}_{n\sigma}^{\dagger} | \text{GS} \rangle$, and obtain a mode-resolved measure D_{kn} of dressing by taking the overlap with $\hat{c}_{k\sigma}^{\dagger} | \text{GS} \rangle$. This measure can be computed from knowledge of p_n , $(y_{dn}, y_{1n}, \dots, y_{Ln})$, and the ground-state covariance matrix $C(| \text{GS} \rangle)$ whose eigenvectors define the natural orbital basis. Where possible, we used NRG to study these quasiparticle-structure-related quantities. However, NRG is inadequate to study more than the first few single-quasiparticle excitations, or to study structure in real space. We overcame these limitations by constructing an ansatz for single-quasiparticle excitations in terms of the natural orbital basis. The important features of this ansatz are (1) that it provides an explicit expression in terms of bare electronic degrees of freedom, for a quasiparticle excitation and (2) that it can be implemented directly on a microscopic model involving an impurity coupled to electrons on a lattice of several thousand sites, rather than on a continuum model discretized on the logarithmic energy grid used in NRG. The ansatz is accurate at affordable computational cost in a regime of well-developed correlations. We further showed that the difference $\delta\rho$ between the density of single-particle states of \hat{H}_{qp} and the actual many-body system is an increasing function of energy at energies approaching or equal to the Kondo temperature. This is a “beyond ideal Fermi-liquid theory” effect. We finally showed that the position resolved dressing \tilde{D}_{jn} decays with a nontrivial power law at large distances.

We envisage that the study we presented here could provide a foundation for the explicit calculation of the single-particle scattering matrix for a quantum impurity imbedded in a nontrivial geometry such as a disordered host or a mesoscopic electronic device. This is a challenging task because the quasiparticle weight z , which appears in the effective Hamiltonian, is determined by the many-body state of the system, which cannot be calculated with methods such as NRG, with its crudely resolved discrete representation of the host. In the present paper, we considered single quasiparticle excitations. The methods we developed may be a good starting point to investigate the weak interactions between two or more quasiparticles. We also suspect that simple modifications to our ansatz could extend its regime of validity. For instance, in the present paper, we determine the natural orbital basis at the start of the calculation, using the ground state as a reference. In our own ongoing study, we are investigating whether it is profitable to adjust the natural orbital basis itself when dealing with excitations. Finally, the fact that natural orbitals are efficient for describing not only the ground state but also excitations, presages the possible future development of natural orbital methods for the challenging problem of nonequilibrium time evolution in quantum impurity systems.

ACKNOWLEDGMENTS

Insightful comments and suggestions from Serge Florens are gratefully acknowledged.

APPENDIX: BENCHMARKING

We benchmark our proposed methods against known results. To gauge generality, we test the natural orbital methods on the SIAM and on another model. The choice of this model is dictated by the demand that it should be sufficiently different from the SIAM to give independent confirmation of the accuracy of the method, yet its structure must be similar enough that computer codes developed for the SIAM can easily be adapted.

1. The interacting resonant level model

The interacting resonant level model (IRLM) is ideal for this purpose. It describes a band of noninteracting, spinless fermions hybridizing with a localized orbital. Additionally there is a local interaction between a particle in the local orbital and one in the adjacent lattice site of the band. We study the particle-hole symmetric version of the Hamiltonian, which reads

$$\hat{H} = U \left(\hat{n}_d - \frac{1}{2} \right) \left(\hat{n}_0 - \frac{1}{2} \right) + V (d^\dagger \psi_0 + \psi_0^\dagger d) + \sum_{k=1}^L \varepsilon_k \hat{c}_k^\dagger \hat{c}_k. \quad (\text{A1})$$

Here \hat{d}^\dagger creates a particle in the localized orbital and $\hat{\psi}_0^\dagger$ creates a particle on the lattice site adjacent to the impurity. Furthermore

$$\hat{n}_d = \hat{d}^\dagger \hat{d}, \quad \hat{\psi}_0 = \frac{1}{\sqrt{L}} \sum_{k=1}^L \hat{c}_k, \quad \hat{n}_0 = \hat{\psi}_0^\dagger \hat{\psi}_0. \quad (\text{A2})$$

We take the Fermi energy to be at zero, in the middle of the band. As in the SIAM, hybridization is quantified by the spectral density $\Delta = \pi V^2 / 2D$ at the Fermi level, of the operator $V \hat{\psi}_0$ in the infinite system uncoupled from the impurity. In the $\Delta \ll D$ regime, and for $U < 0$, the IRLM hosts the same physics as the Kondo model, in which there is a local exchange interaction between the magnetic moment of a spin-1/2 impurity and nearby conduction band electrons. (There is a mapping between the spin degrees of freedom in the Kondo model and the IRLM, the charge degrees of the Kondo model being spectators that do not couple to the impurity [52–54].) The quantum phase transition seen in the Kondo model when the exchange interaction switches from ferro- to antiferromagnetic, translates to a critical point in the IRLM at $U \sim -D$. Increasing U beyond the critical point corresponds to increasing the Kondo temperature in the antiferromagnetic regime.

2. Ansatz 2

Apart from the study of Fermi-liquid quasiparticles, we are also interested in establishing if there are any fundamental limitations to applying natural orbital methods to excited state problems. Even though the ansatz formulated in Sec. III will

prove sufficiently accurate for our purposes, we introduce an improved, but more computationally expensive Ansatz 2 for the purpose of comparing to the ansatz of Sec. III, which here we refer to as Ansatz 1.

Ansatz 2 is obtained by relaxing the assumption that when a particle ends up in the unoccupied sector, the particles in the correlated sector are undisturbed. Instead, a particle in the unoccupied sector may be associated to an arbitrary configuration of m particles in the correlated sector. Thus we consider $N + 1$ particle states of the form

$$|p, k\rangle_2 = \sum_{\alpha \in \mathcal{U}} \sum_{\{\alpha_i\}_m} u_{\alpha, \{\alpha_i\}_m, k} \hat{q}_\alpha^\dagger |\{\alpha_i\}_m\rangle + \sum_{\{\alpha_i\}_{m+1}} v_{\{\alpha_i\}_{m+1}, k} |\{\alpha_i\}_{m+1}\rangle. \quad (\text{A3})$$

The optimal coefficients $u_{\alpha, \{\alpha_i\}_m, k}$ and $v_{\{\alpha_i\}_{m+1}, k}$ are found in the same manner as before. They are thus seen to be eigenvectors of the effective Hamiltonian

$$\tilde{H}_p = \begin{pmatrix} \tilde{H}_{\mathcal{U}\mathcal{U}} & \tilde{H}_{\mathcal{U}\mathcal{C}} \\ \tilde{H}_{\mathcal{U}\mathcal{C}}^\dagger & H_{\mathcal{C}\mathcal{C}} \end{pmatrix}, \quad (\text{A4})$$

where the blocks $\tilde{H}_{\mathcal{U}\mathcal{U}}$ and $\tilde{H}_{\mathcal{U}\mathcal{C}}$ are now given by

$$\begin{aligned} [\tilde{H}_{\mathcal{U}\mathcal{U}}]_{(\alpha, \{\alpha_i\}_m), (\beta, \{\beta_i\}_m)} &= \langle \{\alpha_i\}_m | \hat{q}_\alpha^\dagger \hat{H} \hat{q}_\beta^\dagger | \{\beta_i\}_m \rangle, \\ [\tilde{H}_{\mathcal{U}\mathcal{C}}]_{(\alpha, \{\alpha_i\}_m), \{\beta_i\}_{m+1}} &= \langle \{\alpha_i\}_m | \hat{q}_\alpha^\dagger \hat{H} | \{\beta_i\}_{m+1} \rangle, \end{aligned} \quad (\text{A5})$$

while the block $H_{\mathcal{C}\mathcal{C}}$ is the same as before (43). The block $\tilde{H}_{\mathcal{U}\mathcal{U}}$ has dimension $N_{\mathcal{U}} \times \binom{N_{\mathcal{C}}}{m}$, which is considerably larger than the corresponding block (43) in the effective Hamiltonian associated with Ansatz 1.

3. Local density of states of the d orbital

We will explore the accuracy of Ansatz 1 and Ansatz 2 by considering the local density of states (LDOS) of the d orbital, a quantity that is sensitive to single-particle excitations on top of the ground state. The two ansätze that we study were designed to be accurate in the Fermi-liquid regime, i.e., below the Kondo scale. We intentionally choose the LDOS as a benchmark, not only to demonstrate the accuracy of the ansätze in the expected regime, *but also to explore how they break down*. We will see that the LDOS is accurately reproduced at frequencies up to $\sim T_K$, and start breaking down at higher frequencies, where the local Fermi-liquid picture does not apply. We stress that the ansätze studied here, are not being presented to compete with existing methods to compute the LDOS of the d orbital. Instead, they come into their own right when quasiparticles living in the bulk, rather than impurity properties, are considered.

For a finite system, in which the band has L orbitals, the LDOS of the d orbital is given by

$$\begin{aligned} A_L(\omega) &= \frac{1}{\pi} \text{Re} \int_0^\infty dt e^{i\omega t} \langle \text{GS} | \{\hat{d}_\sigma^\dagger(0), \hat{d}_\sigma(t)\} | \text{GS} \rangle \\ &= \sum_n |\langle \text{GS} | \hat{d}_\sigma^\dagger | h, n\sigma \rangle|^2 \delta(E_{h,n} - E_{\text{GS}} + \omega) \\ &\quad + \sum_n |\langle \text{GS} | \hat{d}_\sigma | p, n\sigma \rangle|^2 \delta(E_{p,n} - E_{\text{GS}} - \omega). \end{aligned} \quad (\text{A6})$$

For the SIAM, we assume zero magnetic field, so that a single spin species may be considered. For the IRLM, the spin index σ is dropped. The summations in respectively the second and third lines are over all excited states with one more or fewer particles than the number of particles in the ground state. For results obtained in the logarithmically discretized model, we use a trick called z averaging to mitigate discretization errors at finite frequency [55]. It involves replacing Λ^{-k} in (19) with Λ^{-k+z} for $k = 1, 2, \dots$, and averaging LDOS results over n_z separate calculations, each performed with a different $z = (\zeta - 1/2)/n_z$, $\zeta = 1, 2, \dots, n_z$. Note that with this discretization, the hopping amplitudes t_j along the Wilson chain (21) have to be calculated recursively [16], using arbitrary precision arithmetic.

In order to arrive at a result independent of the discretization scheme, and that is near the LDOS in the thermodynamic limit, the delta peaks of the finite system LDOS must be broadened. We apply the Gaussian broadening prescription that is standard within NRG

$$A(\omega) = \int_{-\infty}^{\infty} d\varepsilon A_L(\varepsilon) \Gamma(\omega, \varepsilon),$$

$$\Gamma(\omega, \varepsilon) = \frac{1}{\sqrt{2\pi}\eta(\varepsilon)} e^{-(\omega-\varepsilon)^2/2\eta(\varepsilon)^2}. \quad (\text{A7})$$

For results obtained in the logarithmically discretized model, we use a width that decreases linearly as the Fermi energy is approached,

$$\eta_{\log}(\varepsilon) = \frac{2|\varepsilon|}{n_z}. \quad (\text{A8})$$

For results obtained in the system discretized on a regular energy grid, we use a constant width equal to half the single-particle level spacing

$$\eta_{\text{lin}}(\varepsilon) = \frac{D}{L}. \quad (\text{A9})$$

If an STM tip is held near the d orbital and a potential ω/e is maintained between tip and sample, the tunneling current between the tip and the d orbital is proportional to $A(\omega)$. We note that the LDOS of the IRLM is still a topic of active study [56].

Here and further below, all NRG results for the LDOS of the d orbital, were obtained with the density matrix NRG (DM-NRG) algorithm [57], which retains full information of the ground state when the LDOS is evaluated at an arbitrary frequency. In order to use the maximum available information about excited states, we employ the Full Hilbert space method [37]. Thus the sum rule $\int_{-\infty}^{\infty} d\omega A_L(\omega) = 1$ is satisfied identically. We imposed particle number conservation during the iterative diagonalization, and retained up to 128 states per particle-number sector, which corresponds to several thousand kept states in total per iteration.

4. Results for the IRLM

First we present results for the IRLM. We calculate $A(\omega)$ at $\Delta = 0.035D$ and $U = -0.5D$. We compare NRG results to results obtained with Ansatz 1 on a regular energy grid of 4801 orbitals. Natural orbitals were calculated using the RGNO algorithm, with a correlated sector containing four

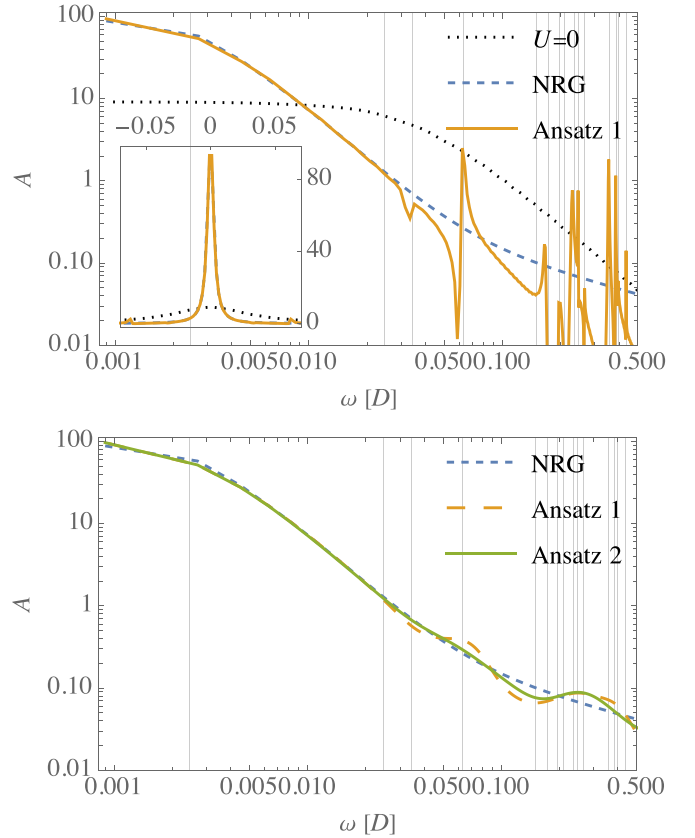


FIG. 8. (Top) Local density of states (LDOS) at the d orbital, for the interacting resonant level model (IRLM), at interaction strength $U = -0.5D$ and hybridization $\Delta = 0.035D$. The main panel shows results in log-log scale. The inset shows the same data in linear scale. The solid curve represents the result obtained with Ansatz 1. The band was discretized on a regular energy grid with 4801 levels. The dashed curve represents an NRG calculation. The dotted curve represents the noninteracting ($U = 0$) result for comparison. Vertical lines indicate the eigenvalues of H_{cc} (43). (Bottom) LDOS of the IRLM at the same parameters $U = -0.5D$ and hybridization $\Delta = 0.035D$ as in the top panel. The NRG data is the same as in the top panel. Results for Ansatz 2 (solid curve) were obtained using the same logarithmic discretization and z averaging as the NRG results. For comparison, results for Ansatz 1 were also recalculated on the logarithmic grid, with z averaging.

particles in $N_c = 8$ orbitals. NRG results were obtained on a Wilson chain of length 52 sites, including the d orbital, with $\Lambda = 1.5$, leading to an infrared cutoff energy $\sim 4 \times 10^{-5}D$. NRG results were z averaged over eight z values. Results are shown in the top panel of Fig. 8, in logarithmic scale, and in linear scale (inset). The peak around $\omega = 0$ is the well-known Kondo resonance. The noninteracting case, $U = 0$, corresponds to the Toulouse point of the anisotropic Kondo model, and therefore still shows a Kondo resonance (of half-width $\Delta = 0.035D$). We see that at $U = -0.5D$, the resonance is about 10 times narrower. This significant downward renormalization of the hybridization proves that we are in the strongly correlated regime. We see that Ansatz 1 implemented on a regular energy grid reproduces the LDOS well, from the Fermi energy up to the point where it has decayed to about 1% of its value at the Fermi energy. It therefore captures low-energy

excitations well, even beyond the Kondo scale (half-width of the Kondo resonance). The eventual breakdown occurs as follows. The effective Hamiltonian (42) describes the hybridization of a (near) continuum of bare single-particle excitations in the unoccupied sector with a discrete spectrum of few-body correlated states in the correlated sector. This discrete spectrum comprises the eigenvalues of the lower-right block H_{CC} of H_p in Eq. (42) (together with the eigenvalues of the particle-hole conjugate, representing one-hole excitations). In Fig. 8, we plot vertical lines representing this discrete spectrum. We see that Ansatz 1 hybridizes the two few-body states that have energies closest above and below the Fermi energy, with the continuum of bare particle and bare hole excitations, to produce a smooth spectral density in the vicinity of the Kondo resonance. The remaining few-body correlated states have energies that lie in the tail of the Kondo resonance. Ansatz 1 does not produce the correct hybridization of these states with the bare particle and hole continua, as seen from the abrupt features of the resulting spectral density in the vicinity of the vertical lines in the tails of the Kondo resonance. While this analysis indicates that Ansatz 1 is sufficiently accurate to allow us to investigate the structure of local Fermi-liquid quasiparticles, we would nonetheless like to see if we cannot improve accuracy at higher frequencies.

As we explained above, Ansatz 2 is too computationally expensive to deploy on a large regular energy grid. In the bottom panel of Fig. 8, we compare Ansatz 1 and Ansatz 2 to NRG results, where now all calculations are performed for the IRLM discretized on the logarithmic grid, and then z averaged. We again use the RGNO algorithm, involving a correlated sector of $N_C = 8$ orbitals, containing four particles. The interaction strength U and hybridization Δ are the same as in the top panel. As might be expected, z averaging, together with the increased broadening (A8) at intermediate energies, compared to (A9), smoothes the spurious abrupt features in the LDOS obtained by means of Ansatz 1. Nonetheless, in the bottom panel of Fig. 3, Ansatz 1 still shows deviations from the NRG result that stand in one to one correspondence with those seen in the top panel, for $|\omega| > 0.025D$. Ansatz 2 significantly mitigates the lowest frequency deviations and remains accurate up to $|\omega| \sim 0.1D$, describing the LDOS of the IRLM well over almost three decades. The benchmarking exercise thus proves that natural orbital methods are in principle suitable to study low-energy excitations of fermionic quantum impurity models. We therefore proceed to our primary system of interest, the single impurity Anderson model (SIAM).

5. Results for the SIAM

As in Sec. V, we study the particle-hole symmetric version of the model (1) where $\varepsilon_d = -U/2$. The LDOS of the d orbital shows a resonance with a width $\tilde{\Delta} = z\Delta$, comparable to $T_K \ll U$, associated with spin fluctuations. Without the Coulomb repulsion $U\hat{n}_{d\uparrow}\hat{n}_{d\downarrow}$, this Kondo resonance is absent, and the LDOS has two peaks at $\omega = \pm\varepsilon_d$ instead. In the presence of Coulomb repulsion, these turn into shoulders at the base of the Kondo resonance, or even (broad) side peaks, at a scale $\varepsilon_d = -U/2$ and $U + \varepsilon_d = U/2$, associated with charge fluctuations. We take $\Delta = 0.09D$ and $U = 0.6D$, for which we compute $T_K = 0.013D$. We perform all calculations on a

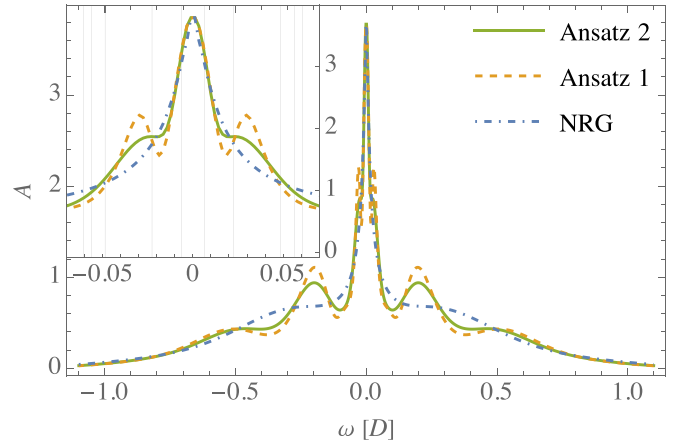


FIG. 9. The local density of states (LDOS) at the d orbital, for the symmetric single impurity Anderson model (SIAM) with $\Delta = 0.09D$ and $U = 0.6D$. The main panel shows the result over a frequency window that spans the whole band. The inset zooms in on the Kondo resonance. The vertical lines in the inset represent the eigenvalues of H_{CC} (43). Results for Ansatz 1 and Ansatz 2 were obtained employing the same logarithmic discretization and z averaging as in NRG.

logarithmic grid, and employ z averaging over $n_z = 8$ values of z . We employed a Wilson chain of length $L = 51$ sites, with $\Lambda = 2$. Natural orbitals were obtained with the RGNO algorithm. A correlated sector with $N_C = 12$ orbitals (six spin up and six spin down), containing three spin up and three spin down electrons was used. The RGNO algorithm could determine the ground-state energy to an error of $\sim 5\%$ of the Kondo temperature, meaning that we may expect Kondo physics to be described accurately. We note that the accuracy of the ground-state calculation is easily improved by increasing the size of the correlated sector. However, the enlarged correlated sector significantly slows down the subsequent calculation of

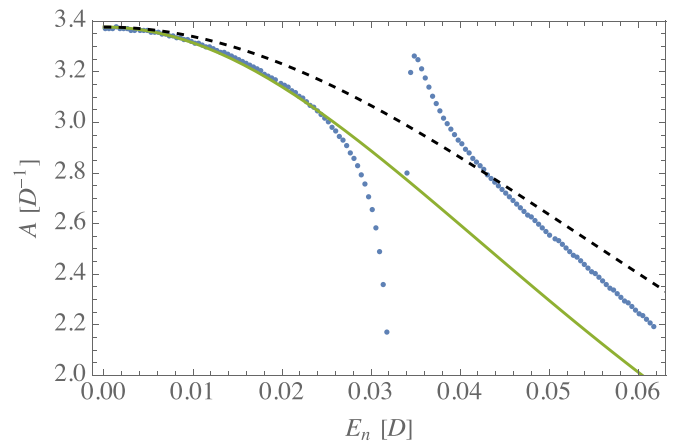


FIG. 10. The LDOS of the d orbital (A6) as calculated with the ansatz (dots), for the symmetric SIAM with $\Delta = 0.09D$ and $U = 0.2D$, calculated on a regular energy grid with $L = 4801$ orbitals. The solid line represents the Lorentzian LDOS $z^2 \Delta / \pi (\omega^2 + z^2 \Delta^2)$, with z estimated from the low-energy spectrum obtained with NRG. The dashed line represents the unrenormalized $z = 1$ Lorentzian LDOS at the same Δ .

excited states. We have therefore settled for the minimum accuracy that is sufficient for the excited state calculation. In Fig. 9 we compare NRG results for the LDOS of the d orbital, to results obtained using Ansatz 1 and Ansatz 2. The NRG results show a clear Kondo resonance of half-width $\sim 0.02D$ and broad shoulders associated with the scale $U/2 = 0.3D$. Both Ansatz 1 and Ansatz 2 reproduce the general shape well and are quantitatively accurate at low frequencies. The inset to Fig. 1 shows a zoom of the central peak of the LDOS, with vertical lines indicating the eigenenergies of $H_{C,C}$ (43). As in the case of the IRLM, Ansatz 1 and Ansatz 2 both handle the hybridization of the two few-body correlated eigenstates of $H_{C,C}$ that are closest in energy to the Fermi level well (the two vertical lines at $\pm 0.006D$). Again, deviations from NRG results are associated with higher excited few-body correlated states, for instance those represented by the vertical lines at $\pm 0.02D$. Ansatz 2 mitigates these deviations compared to Ansatz 1, but errors at this frequency scale are still on the order of 5% for Ansatz 2.

At this point we conclude our study of Ansatz 2. Benchmarking shows that Ansatz 1 is accurate in the Fermi liquid regime below T_K . It remains to check Ansatz 1 for the SIAM discretized on the large regular energy grid necessary for obtaining real space resolution at the scale of the Fermi wavelength. Here we find that results are less accurate than on the Wilson chain. To obtain a quantitatively accurate LDOS on a regular energy grid with 4801 levels at $\Delta = 0.09$, we had to reduce the interaction strength to $U = 0.2D$. This gives a quasiparticle weight $z = 0.77$, which still represents a finite renormalization. In Fig. 10 we show the low-energy LDOS computed with the ansatz, compared to what it should be for $z = 0.77$. We see good agreement up to $\omega = 0.02D$, and a breakdown at $\omega = 0.03D$. Here $T_K = 0.064D$. From various trial calculations we performed with the ansatz, we believe that the energy range in which the ansatz is accurate would be extended, if we could use a larger correlated sector, but that would make the calculation too expensive computationally, to perform in a reasonable time.

-
- [1] R. Shankar, Renormalization-group approach to interacting fermions, *Rev. Mod. Phys.* **66**, 129 (1994).
 - [2] A. C. Hewson, *The Kondo Problem to Heavy Fermions* (Cambridge University Press, Cambridge, 1993).
 - [3] M. Pustilnik and L. Glazman, Kondo effect in quantum dots, *J. Phys.: Condens. Matter* **16**, R513 (2004).
 - [4] A. Georges, G. Kotliar, W. Krauth, and M. J. Rozenberg, Dynamical mean-field theory of strongly correlated fermion systems and the limit of infinite dimensions, *Rev. Mod. Phys.* **68**, 13 (1996).
 - [5] E. Eidelstein, E. Gull, and G. Cohen, Multiorbital quantum impurity solver for general interactions and hybridizations, *Phys. Rev. Lett.* **124**, 206405 (2020).
 - [6] N.-O. Linden, M. Zingl, C. Hubig, O. Parcollet, and U. Schollwöck, Imaginary-time matrix product state impurity solver in a real material calculation: Spin-orbit coupling in Sr_2RuO_4 , *Phys. Rev. B* **101**, 041101(R) (2020).
 - [7] D. Werner, J. Lotze, and E. Arrigoni, Configuration interaction based nonequilibrium steady state impurity solver, *Phys. Rev. B* **107**, 075119 (2023).
 - [8] A. Erpenbeck, W.-T. Lin, T. Blommel, L. Zhang, S. Isakov, L. Bernheimer, Y. Núñez Fernández, G. Cohen, O. Parcollet, X. Waintal, and E. Gull, Tensor train continuous time solver for quantum impurity models, *Phys. Rev. B* **107**, 245135 (2023).
 - [9] B. Kloss, J. Thoenniss, M. Sonner, A. Lerose, M. T. Fishman, E. M. Stoudenmire, O. Parcollet, A. Georges, and D. A. Abanin, Equilibrium quantum impurity problems via matrix product state encoding of the retarded action, [arXiv:2306.17216](https://arxiv.org/abs/2306.17216).
 - [10] J. E. Gubernatis, J. E. Hirsch, and D. J. Scalapino, Spin and charge correlations around an Anderson magnetic impurity, *Phys. Rev. B* **35**, 8478 (1987).
 - [11] V. Barzykin and I. Affleck, The Kondo screening cloud: What can we learn from perturbation theory? *Phys. Rev. Lett.* **76**, 4959 (1996).
 - [12] L. Borda, Kondo screening cloud in a one-dimensional wire: Numerical renormalization group study, *Phys. Rev. B* **75**, 041307(R) (2007).
 - [13] B. Lechtenberg and F. B. Anders, Spatial and temporal propagation of Kondo correlations, *Phys. Rev. B* **90**, 045117 (2014).
 - [14] S. Florens and I. Snyman, Universal spatial correlations in the anisotropic Kondo screening cloud: Analytical insights and numerically exact results from a coherent state expansion, *Phys. Rev. B* **92**, 195106 (2015).
 - [15] M. Debertolis, I. Snyman, and S. Florens, Simulating realistic screening clouds around quantum impurities: Role of spatial anisotropy and disorder, *Phys. Rev. B* **106**, 125115 (2022).
 - [16] R. Bulla, T. A. Costi, and T. Pruschke, Numerical renormalization group method for quantum impurity systems, *Rev. Mod. Phys.* **80**, 395 (2008).
 - [17] K. G. Wilson, The renormalization group: Critical phenomena and the Kondo problem, *Rev. Mod. Phys.* **47**, 773 (1975).
 - [18] P. Nozières, A “Fermi-liquid” description of the Kondo problem at low temperatures, *J. Low Temp. Phys.* **17**, 31 (1974).
 - [19] H. R. Krishna-Murthy, J. W. Wilkins, and K. G. Wilson, Renormalization-group approach to the Anderson model of dilute magnetic alloys. I. Static properties for the symmetric case, *Phys. Rev. B* **21**, 1003 (1980).
 - [20] A. C. Hewson, Renormalized perturbation expansions and Fermi liquid theory, *Phys. Rev. Lett.* **70**, 4007 (1993).
 - [21] A. C. Hewson, A. Oguri, and D. Meyer, Renormalized parameters for impurity models, *Eur. Phys. J. B* **40**, 177 (2004).
 - [22] C. Mora, C. P. Moca, J. von Delft, and G. Zaránd, Fermi-liquid theory for the single-impurity Anderson model, *Phys. Rev. B* **92**, 075120 (2015).
 - [23] M. Filippone, C. P. Moca, A. Weichselbaum, J. von Delft, and C. Mora, At which magnetic field, exactly, does the Kondo resonance begin to split? A Fermi liquid description of the low-energy properties of the Anderson model, *Phys. Rev. B* **98**, 075404 (2018).
 - [24] V. Dobrosavljević, T. R. Kirkpatrick, and B. G. Kotliar, Kondo effect in disordered systems, *Phys. Rev. Lett.* **69**, 1113 (1992).
 - [25] G. Zaránd and L. Udvardi, Enhancement of the Kondo temperature of magnetic impurities in metallic point contacts due to the

- fluctuations of the local density of states, *Phys. Rev. B* **54**, 7606 (1996).
- [26] I. Aleiner, P. Brouwer, and L. Glazman, Quantum effects in Coulomb blockade, *Phys. Rep.* **358**, 309 (2002).
- [27] R. K. Kaul, G. Zaránd, S. Chandrasekharan, D. Ullmo, and H. U. Baranger, Spectroscopy of the Kondo problem in a box, *Phys. Rev. Lett.* **96**, 176802 (2006).
- [28] D. Ullmo, Many-body physics and quantum chaos, *Rep. Prog. Phys.* **71**, 026001 (2008).
- [29] D. E. Liu, S. Burdin, H. U. Baranger, and D. Ullmo, Mesoscopic Anderson box: Connecting weak to strong coupling, *Phys. Rev. B* **85**, 155455 (2012).
- [30] D. Ullmo, D. E. Liu, S. Burdin, and H. U. Baranger, Mesoscopic fluctuations in the Fermi-liquid regime of the Kondo problem, *Eur. Phys. J. B* **86**, 353 (2013).
- [31] V. G. Miranda, L. G. G. V. Dias da Silva, and C. H. Lewenkopf, Disorder-mediated Kondo effect in graphene, *Phys. Rev. B* **90**, 201101(R) (2014).
- [32] K. Slevin, S. Kettmann, and T. Ohtsuki, Multifractality and the distribution of the Kondo temperature at the Anderson transition, *Eur. Phys. J. B* **92**, 281 (2019).
- [33] B. Brun, F. Martins, S. Faniel, B. Hackens, G. Bachelier, A. Cavanna, C. Ulysse, A. Ouerghi, U. Gennser, D. Mailly, S. Huan, V. Bayot, M. Sanquer, and H. Sellier, Wigner and Kondo physics in quantum point contacts revealed by scanning gate microscopy, *Nat. Commun.* **5**, 4290 (2014).
- [34] K. Kolasinski, B. Szafran, B. Brun, and H. Sellier, Interference features in scanning gate conductance maps of quantum point contacts with disorder, *Phys. Rev. B* **94**, 075301 (2016).
- [35] B. Brun, F. Martins, S. Faniel, B. Hackens, A. Cavanna, C. Ulysse, A. Ouerghi, U. Gennser, D. Mailly, P. Simon, S. Huan, V. Bayot, M. Sanquer, and H. Sellier, Electron phase shift at the zero-bias anomaly of quantum point contacts, *Phys. Rev. Lett.* **116**, 136801 (2016).
- [36] I. Affleck, The Kondo screening cloud: What it is and how to observe it, in *Perspectives of Mesoscopic Physics*, edited by A. Aharony and O. Entin-Wohlman (World Scientific, Singapore, 2010), pp. 1–44.
- [37] R. Peters, T. Pruschke, and F. B. Anders, Numerical renormalization group approach to Green's functions for quantum impurity models, *Phys. Rev. B* **74**, 245114 (2006).
- [38] A. Weichselbaum and J. von Delft, Sum-rule conserving spectral functions from the numerical renormalization group, *Phys. Rev. Lett.* **99**, 076402 (2007).
- [39] S. Bravyi and D. Gosset, Complexity of quantum impurity problems, *Commun. Math. Phys.* **356**, 451 (2017).
- [40] M. Debertolis, S. Florens, and I. Snyman, Few-body nature of Kondo correlated ground states, *Phys. Rev. B* **103**, 235166 (2021).
- [41] P.-O. Löwdin, Quantum theory of many-particle systems. I. Physical interpretations by means of density matrices, natural spin-orbitals, and convergence problems in the method of configurational interaction, *Phys. Rev.* **97**, 1474 (1955).
- [42] E. R. Davidson, Properties and uses of natural orbitals, *Rev. Mod. Phys.* **44**, 451 (1972).
- [43] J. Olsen, The CASSCF method: A perspective and commentary, *Int. J. Quantum Chem.* **111**, 3267 (2011).
- [44] X. Li and J. Paldus, Recursive generation of natural orbitals in a truncated orbital space, *Int. J. Quantum Chem.* **105**, 672 (2005).
- [45] F. Aikebaier, T. Ojanen, and J. L. Lado, Extracting electronic many-body correlations from local measurements with artificial neural networks, *SciPost Phys. Core* **6**, 030 (2023).
- [46] T. I. Vanhala and T. Ojanen, Complexity of fermionic states, [arXiv:2306.07584](https://arxiv.org/abs/2306.07584).
- [47] D. Zgid, E. Gull, and G. K.-L. Chan, Truncated configuration interaction expansions as solvers for correlated quantum impurity models and dynamical mean-field theory, *Phys. Rev. B* **86**, 165128 (2012).
- [48] R.-Q. He and Z.-Y. Lu, Quantum renormalization groups based on natural orbitals, *Phys. Rev. B* **89**, 085108 (2014).
- [49] P. W. Anderson, Localized magnetic states in metals, *Phys. Rev.* **124**, 41 (1961).
- [50] C. J. Turner, K. Meichanetzidis, Z. Papić, and J. K. Pachos, Optimal free descriptions of many-body theories, *Nat. Commun.* **8**, 14926 (2017).
- [51] C. Lin and A. A. Demkov, Efficient variational approach to the impurity problem and its application to the dynamical mean-field theory, *Phys. Rev. B* **88**, 035123 (2013).
- [52] F. Guinea, V. Hakim, and A. Muramatsu, Bosonization of a two-level system with dissipation, *Phys. Rev. B* **32**, 4410 (1985).
- [53] G. Kotliar and Q. Si, Toulouse points and non-Fermi-liquid states in the mixed-valence regime of the generalized Anderson model, *Phys. Rev. B* **53**, 12373 (1996).
- [54] T. A. Costi and G. Zaránd, Thermodynamics of the dissipative two-state system: A Bethe-ansatz study, *Phys. Rev. B* **59**, 12398 (1999).
- [55] W. C. Oliveira and L. N. Oliveira, Generalized numerical renormalization-group method to calculate the thermodynamical properties of impurities in metals, *Phys. Rev. B* **49**, 11986 (1994).
- [56] G. Camacho, P. Schmitteckert, and S. T. Carr, Local density of states of the interacting resonant level model at zero temperature, *Phys. Rev. B* **105**, 075116 (2022).
- [57] W. Hofstetter, Generalized numerical renormalization group for dynamical quantities, *Phys. Rev. Lett.* **85**, 1508 (2000).